Geophysical and Astrophysical Fluid Dynamics
Vol. 00, No. 00, February 2006, 1–30

Nonlocal memory effects of the electromotive force by fluid motion with helicity and two-dimensional periodicity

Kumiko Hori* and Shigeo Yoshida

Department of Earth and Environmental Sciences, Graduate School of Environmental Studies, Nagoya University, Furo-cho, Chikusa-ku, 464-8601 Nagoya, Japan

(*Received 24 August 2007; in final form 28 March 2008*)

In mean-field dynamo theory, the electromotive force term $\langle \mathbf{u}' \times \mathbf{B}' \rangle$ due to small-scale fields connects the small-scale magnetic field with the large-scale field. This term is usually approximated as the α-effect, assumed to be instantaneous in time and local in space. However, the approximation is valid only when the magnetic Reynolds number Rm is much less than unity, and is inappropriate when $Rm \gtrsim 1$, which is the condition satisfied in the Earth's core or solar convection zone. We introduce a function ϕ_{qr} as a nonlocal and non-instantaneous generalization of the usual α-effect and examine its behaviour as a function of Rm in the range $1/64 \leq Rm \leq 10$ for a kinematic dynamo model. We use the flow of G.O.Roberts (1972), which is steady and has non-zero helicities and two-dimensional periodicity. As a result, we identify three regions in Rm space according to the behaviour of the function ϕ_{qr}: (i) $Rm \lesssim 1/4$, where the function ϕ_{qr} is local and instantaneous and can be approximated by the traditional α and β effects, (ii) $1/4 \lesssim Rm \lesssim 4$, where the deviation from the traditional α and β effects increases and nonlocalness and non-instantaneousness increase, and (iii) $Rm \gtrsim 4$, where boundary layers develop fully and nonlocalness and non-instantaneousness are prominent. We show that the nonlocal memory effect for $Rm \gtrsim 4$ strongly affects the dynamo action and explains an observed augmentation of the growth rate in the dispersion relation. The results imply that the nonlocal memory effect of the electromotive force should be important in the geodynamo or the solar dynamo.

KEY WORDS: mean-field dynamo theory, α-effect, electromotive force, magnetic Reynolds number, nonlocal memory effect

1 Introduction

Mean-field theory is a useful tool for interpreting the generation of dynamos. The generation of the magnetic field $\mathbf{B}$ is described in magnetohydrodynamics (MHD) by the induction equation:

$$\frac{\partial \mathbf{B}}{\partial t} = \nabla \times (\mathbf{u} \times \mathbf{B}) + Rm^{-1} \nabla^2 \mathbf{B}, \tag{1}$$

where $\mathbf{u}$ is the fluid velocity and $Rm = \mathcal{U}\mathcal{L}/\lambda$ is the magnetic Reynolds number with λ being the magnetic diffusivity, $\mathcal{L}$ the characteristic length and $\mathcal{U}$ the characteristic velocity. Here t denotes time nondimensionalised by the advection time scale $\tau_{\rm a} = \mathcal{L}/\mathcal{U}$. The magnetic Reynolds number Rm is the ratio of the diffusion time $\tau_{\rm d} = \mathcal{L}^2/\lambda$ to the advection time $\tau_{\rm a}$ and expresses how much the magnetic lines of force can be distorted. Its order of magnitude is $Rm = \mathrm{O}(10^{0-2})$ for the Earth and $Rm > \mathrm{O}(10^5)$ for the Sun. In mean-field theory, it is considered that the fluid velocity $\mathbf{u}$ and the magnetic field $\mathbf{B}$ can be separated into the mean parts, $\langle \mathbf{u} \rangle$ and $\langle \mathbf{B} \rangle$, and the fluctuating parts, $\mathbf{u}'$ and $\mathbf{B}'$. The mean part of (1) becomes

$$\frac{\partial \langle \mathbf{B} \rangle}{\partial t} - \nabla \times (\langle \mathbf{u} \rangle \times \langle \mathbf{B} \rangle) - Rm^{-1} \nabla^2 \langle \mathbf{B} \rangle = \nabla \times \boldsymbol{\mathcal{E}}, \tag{2}$$

*Corresponding author. Email: hori@eps.nagoya-u.ac.jp

Geophysical and Astrophysical Fluid Dynamics
ISSN 0309-1929 print/ ISSN 1029-0419 online
http://www.tandf.co.uk/journals
DOI: 10.1080/03091920xxxxxxxxx

where

$$\boldsymbol{\mathcal{E}} = \langle \mathbf{u}' \times \mathbf{B}' \rangle. \tag{3}$$

The fluctuating part is obtained by subtracting (2) from (1):

$$\frac{\partial \mathbf{B}'}{\partial t} - \nabla \times (\langle \mathbf{u} \rangle \times \mathbf{B}') - \nabla \times (\mathbf{u}' \times \mathbf{B}') + \nabla \times \boldsymbol{\mathcal{E}} - Rm^{-1} \nabla^2 \mathbf{B}' = \nabla \times (\mathbf{u}' \times \langle \mathbf{B} \rangle). \tag{4}$$

In mean-field theory, the generation of magnetic fields is understood in terms of the interaction between small-scale phenomena (4) and large-scale phenomena (2). The effect of small-scale fields on the large-scale magnetic field is represented by the electromotive force $\boldsymbol{\mathcal{E}}$, which acts as the source of the mean field $\langle \mathbf{B} \rangle$. On the other hand, (4) expresses the generation of a small-scale field $\mathbf{B}'$ by the mean field $\langle \mathbf{B} \rangle$, if we regard the right-hand side as the source term. Note that (4) allows non-zero $\mathbf{B}'$ even if $\langle \mathbf{B} \rangle = \mathbf{0}$. This is called the small-scale dynamo (e.g. Rädler 2000, Desjardins *et al.* 2007, Tobias and Weiss 2007). However, we neglect this component and only deal with $\mathbf{B}'$ induced by the mean field $\langle \mathbf{B} \rangle$.

The key in mean-field theory is how the electromotive force term $\boldsymbol{\mathcal{E}}$ is expressed as a functional of the mean field $\langle \mathbf{B} \rangle$. It can be seen from (4) that the fluctuating field $\mathbf{B}'$ is a linear functional of the mean field $\langle \mathbf{B} \rangle$. if we regard the right-hand side as the source term of the equation. It follows that the electromotive force $\boldsymbol{\mathcal{E}}$ is also a linear functional of the mean field $\langle \mathbf{B} \rangle$. Its general form should therefore be written as

$$\mathcal{E}_q(\mathbf{x}, t) = \int_{-\infty}^{t} \int_{-\infty}^{\infty} \phi_{qr}(\mathbf{x} - \boldsymbol{\xi}, t - \tau) \langle B \rangle_r(\boldsymbol{\xi}, \tau) \mathrm{d}\boldsymbol{\xi} \mathrm{d}\tau \quad (q, r = 1, 2, 3) \tag{5}$$

if the average properties of the velocity field is stationary and uniform (e.g. P.H.Roberts 1994, Rädler 2000). Here ϕ_{qr} is the kernel of the functional. The kernel is usually approximated as local and instantaneous. This approximation allows the electromotive force term to be written in the form of a Taylor series as

$$\mathcal{E}_q(\mathbf{x}, t) = \alpha_{qr} \langle B \rangle_r(\mathbf{x}, t) + \beta_{qrs} \frac{\partial \langle B \rangle_r(\mathbf{x}, t)}{\partial x_s} + ... \quad (q, r = 1, 2, 3) \tag{6}$$

(e.g. Steenbeck *et al.* 1966, Krause and Rädler 1980), where α_{qr} and β_{qrs} are constant tensor elements. Decomposition of the α and magnetic-field-gradient tensors into symmetric and antisymmetric parts yields

$$\mathcal{E}_q = \alpha_{qr}^{(\mathrm{s})} \langle \mathbf{B} \rangle_r + [\boldsymbol{\gamma} \times \langle \mathbf{B} \rangle]_q - \beta_{qr}^{(\mathrm{s})} [\nabla \times \langle \mathbf{B} \rangle]_r - [\boldsymbol{\delta} \times (\nabla \times \langle \mathbf{B} \rangle)]_q - \kappa_{qrs} (\nabla \langle \mathbf{B} \rangle)_{rs}^{(\mathrm{s})} \tag{7}$$

(Rädler 2000), where $\alpha_{qr}^{(\mathrm{s})}$ and $\beta_{qr}^{(\mathrm{s})}$ are symmetric tensors, $\boldsymbol{\gamma}$ and $\boldsymbol{\delta}$ are vectors, κ_{qrs} is a third-rank tensor and $(\nabla \langle \mathbf{B} \rangle)^{(\mathrm{s})}$ is the symmetric part of the gradient tensor of $\langle \mathbf{B} \rangle$. Here, terms including second or higher-order derivatives of $\langle \mathbf{B} \rangle$ are neglected.

For isotropic small-scale fields, (7) reduces to

$$\boldsymbol{\mathcal{E}}(\mathbf{x}, t) = \alpha \langle \mathbf{B} \rangle(\mathbf{x}, t) - \beta \nabla \times \langle \mathbf{B} \rangle(\mathbf{x}, t), \tag{8}$$

where α and β are constants. The effect of the term containing α is called the α-effect, and represents the generation of a large-scale field. The second term containing β is called the β-effect, and represents the dissipation of the large-scale field. The coefficients α and β are often treated as smooth functions of time and space if the average properties of the velocity field are non-stationary or non-uniform.

Equation (8) is the most commonly used form of the electromotive force and has been useful for explaining kinematic and MHD dynamos. It is known that the α^2-dynamo mechanism or the $\alpha\omega$-dynamo mechanism based on the local and instantaneous α-effect can generate large-scale magnetic fields (e.g. Steenbeck and Krause 1966, P.H.Roberts 1972). Numerical three-dimensional MHD dynamo simulations are therefore often interpreted in terms of the α and β effects (e.g. Kageyama and Sato 1997, Olson *et al.* 1999).

This type of interpretation has recently been used quantitatively. Correlation of the electromotive force and the magnetic field of a numerical simulation is used to determine the coefficients α and β, and the resulting mean field equation is solved to see if the average magnetic field can be reproduced (Brandenburg and Sokoloff 2002, Schrinner *et al.* 2005, Kowal *et al.* 2006, Schrinner *et al.* 2007). These attempts only sometimes succeed.

To summarize, reduction of (5) to (8) has been achieved under three assumptions: isotropy, instantaneousness and localness. However, these assumptions do not hold under some circumstances. Anisotropy is sometimes important for the Earth or Sun, because of the strong influences of rotation and the gravity field. Anisotropy in the form of (7) has been studied extensively (e.g. Rädler 2000). Local numerical simulations have been performed recently to reveal the latitude and depth dependence of the anisotropy in the Earth and Sun (e.g. Matsushima 2005, Käpylä *et al.* 2006).

Our study focuses on the validity of the other two assumptions, localness and instantaneousness. The local and instantaneous approximation is valid only for $Rm \ll 1$ (figure 1), for which the magnetic lines of force are distorted only slightly by a flow. The approximation may break down for $Rm \gtrsim 1$, which is the condition appropriate for a geodynamo or solar dynamo. As Rm increases, the magnetic lines of force are distorted more strongly (figure 1), which gives rise to nonlocal and non-instantaneous effects. The limitations of the approximation have been addressed in past studies on kinematic or magnetohydrodynamic dynamos. For example, G.O.Roberts (1972) numerically solved a kinematic dynamo produced by simplified columnar fluid motion and attempted to explain the results using the α-effect. He found that the local α-effect cannot be used to explain the result for $Rm \gtrsim 1$, in spite of its success for $Rm \ll 1$. Another recent example is the analysis of Schrinner *et al.* (2005, 2007) on numerical MHD dynamo simulations for $Rm \gtrsim 1$. They found that the results cannot be explained only by local and instantaneous α and β effects. These results return us to the general equation (5).

Recent studies have suggested that the introduction of nonlocal or non-instantaneous kernels in the electromotive force strongly affects the resulting magnetic field. Fedotov *et al.* (2002, 2003) assumed a finite correlation time for turbulent flow and examined a non-instantaneous effect, which they called the 'memory effect', on the generation of the mean field. They showed that the memory effect in α suppresses the growth of the mean field, whereas in β it enhances the growth. Their studies, however, were restricted to the local effect and they assumed the form of the non-instantaneous effect to be of the exponential form $\mathrm{e}^{-t/\tau}$ with τ being a correlation time, the validity of which is not obvious. Urpin (2002) calculated the electromotive force caused by an isotropic homogeneous turbulence with a time correlation, but without nonlocal effects. He found that a non-instantaneous β-effect gives rise to a mode which decays with the correlation time of kinetic turbulence. Moreover, Courvoisier *et al.* (2006) calculated the α-effect induced by a time-dependent modified G.O. Roberts' flow, and found that the time-dependence of the fluid motion can change the sign of the α-effect.

It should be noted that the kernel may be non-instantaneous even if the flow is steady. The steadiness of the flow only guarantees that ϕ_{qr} depends on $t - \tau$ as in (5). Two sources exist for the memory effect of the electromotive force $\boldsymbol{\mathcal{E}} = \langle \mathbf{u}' \times \mathbf{B}' \rangle$: the time-dependence of the flow $\mathbf{u}'$ and the time-dependence of the magnetic field $\mathbf{B}'$. We can distinguish them by referring to the former source as the 'kinetic memory effect' and to the latter as the 'magnetic memory effect'. Previous studies (Fedotov *et al.* 2002, 2003, Urpin 2002) considered the kinetic memory effect. In this study, we consider instead the magnetic memory effect, which has never previously been calculated explicitly.

Nonlocal effects have also been shown to contribute significantly to mean-field generation (Rädler *et al.* 1997, Rädler and Brandenburg 2003, Brandenburg and Sokoloff 2002, Kowal *et al.* 2006). Brandenburg and Sokoloff (2002) analysed numerical MHD simulations of the accretion disc to determine the coefficients α and β. They compared direct numerical simulations with mean-field simulations under two different assumptions for the coefficients: a local, non-uniform assumption and a nonlocal, uniform assumption. They showed that the α- and β-effects under the latter assumption can better reproduce the features of direct MHD simulations, suggesting the importance of nonlocal behaviour. However, they considered only nonlocal effects and neglected non-instantaneous effects.

The purpose of this study is to examine both nonlocal and magnetic memory effects for a simple kinematic dynamo. We use a simple dynamo model because discriminating the two effects is difficult for realistic

MHD dynamo simulations. We choose the two-dimensional periodic flow of G.O.Roberts (1972) for the kinematic dynamo model for the following three reasons. First, Roberts' flow has a columnar structure similar to those expected for thermal convection in a rapidly rotating system (e.g. Busse 1970, 2002). Second, the flow shows dynamo action, and a local and instantaneous α-effect has explicitly been verified for $Rm \ll 1$. Third, the two-dimensional periodicity of the flow allows us to define the horizontal average rigorously and to avoid non-uniformity. We return to (5) in this paper and investigate the kinematic dynamo of G.O.Roberts (1972) for $Rm \gtrsim 1$ in terms of the nonlocal and non-instantaneous kernel ϕ_{qr}, which we shall show is necessary for understanding the behaviour of its dispersion relation. The concept behind dynamo experiments recently carried out in Karlsruhe (Stieglitz and Müller 2001, Müller and Stieglitz 2002) originates from Roberts' dynamo model, and much work has been done in interpreting the experimental results (e.g. Rädler *et al.* 2002, Rädler and Brandenburg 2003).

In section 2, we briefly review the settings and results of G.O.Roberts (1972) and clarify the conditions under which the local α-effect is insufficient to interpret the dispersion curve. In section 3, we introduce and formulate the nonlocal and non-instantaneous electromotive force for Roberts' problem. We then present the results of the calculations of the nonlocal and non-instantaneous kernel ϕ_{qr} in (5) in section 4. We show that the kernel exhibits increasingly nonlocal and non-instantaneous behaviour with an increase in Rm for $1/4 \lesssim Rm \lesssim 4$ and that nonlocalness and non-instantaneousness are established for $Rm \gtrsim 4$. We consider the effects of nonlocalness and non-instantaneousness on the dispersion relation of the mean field in section 5 and present an illustrative interpretation of the behaviour of Roberts' solution. Finally, we summarize the results in section 6.

2 G.O. Roberts' problem

G.O.Roberts (1972) investigated a kinematic dynamo problem driven by a fluid motion with a non-zero helicity and two-dimensional periodicity:

$$\mathbf{u}(x,y) = (\sin y, \sin x, \cos x - \cos y) \tag{9}$$

(figure 2). The flow is periodic in the x and y directions: $\mathbf{u}(x+2n\pi, y+2m\pi) = \mathbf{u}(x,y)$ where n and m are integers. Since the helicity of the flow $\langle \mathbf{u} \cdot (\nabla \times \mathbf{u}) \rangle$ is positive, a negative α-effect is expected from the first-order smoothing approximation (e.g. Moffatt 1978). Under Bloch's theorem, the eigenfunctions should have the form

$$\mathbf{B}(\mathbf{x},t) = \mathbf{H}(x,y;\mathbf{j},p)\mathrm{e}^{pt+\mathrm{i}\mathbf{j}\cdot\mathbf{x}}, \tag{10}$$

where $\mathbf{H}$ has the same periodicity as the flow $\mathbf{u}$, *i.e.* $\mathbf{H}(x+2n\pi, y+2m\pi) = \mathbf{H}(x,y)$. Here Roberts considered only the case in which the direction of the Bloch wavenumber $\mathbf{j}$ is the same as that of the axis of the columnar flow:

$$\mathbf{j} = j\mathbf{e}_z, \tag{11}$$

where $\mathbf{e}_z$ is the unit vector in the z direction. Tilgner and Busse (1995) and Plunian and Rädler (2002a) examined the solutions without the assumption (11) and found that the growth rate is largest when the condition (11) is satisfied for any Rm. We thus use the assumption (11) in the following.

Since the flow (9) depends on x and y and is spatially periodic with period 2π, we define the average part as

$$\langle f \rangle(z,t) = \frac{1}{4\pi^2} \int_0^{2\pi} \int_0^{2\pi} f(x,y,z,t)\mathrm{d}x\mathrm{d}y \tag{12}$$

and the fluctuating part as

$$f'(x,y,z,t) = f(x,y,z,t) - \langle f\rangle(z,t), \quad \langle f'\rangle = 0, \tag{13}$$

where f is an arbitrary spatially periodic function with a period of 2π. It naturally follows that the mean flow is zero:

$$\langle \mathbf{u}\rangle = \mathbf{0}. \tag{14}$$

The electromotive force $\boldsymbol{\mathcal{E}}$ becomes a function of z and t from the definition (3) and the definition of the average (12). Since the right-hand side of the z component of (2) vanishes for the above definition of the average, the mean field $\langle B_z\rangle$ eventually vanishes and is not of interest. Thus we set it to zero as

$$\langle B_z\rangle = 0. \tag{15}$$

Substituting (10) into (12) gives

$$\langle \mathbf{B}\rangle(z,t) = \langle \mathbf{H}\rangle(j,p)\mathrm{e}^{pt+\mathrm{i}jz}. \tag{16}$$

Hence the mean field is independent of x and y with a zero z component. Subtracting (16) from (10), we obtain the fluctuating part,

$$\mathbf{B}'(x,y,z,t) = \mathbf{H}'(x,y;j,p)\mathrm{e}^{pt+\mathrm{i}jz}. \tag{17}$$

Roberts numerically calculated the dispersion relations and found that the kinematic problem has at least one growing solution for any Rm. Figure 3 shows the maximum eigenvalue p, which is always pure real, in (Rm, j) space. We can see from this figure that the growth rate is positive for any Rm if the wavenumber j is small. This means that the flow (9) exhibits dynamo action for any Rm.

Figure 4 shows the dispersion relation for two values of Rm. The growth rate $\mathrm{Re}[p]$ for the branch with the largest $\mathrm{Re}[p]$ increases linearly with j for $j \ll 1$ for both values of Rm. This explains why dynamo action always occurs for small j. Roberts implicitly showed that mean-field theory based on the local and instantaneous α-effect can explain the linear behaviour of $\mathrm{Re}[p]$ versus j for small j. Under the local and instantaneous approximation for the α- and β-effects, a two-dimensional variant of (8) holds. With eigenfunctions of the forms (16) and (17) the variant becomes

$$\widetilde{\boldsymbol{\mathcal{E}}}(j,p) \sim \alpha\langle \mathbf{H}\rangle - \mathrm{i}j\beta\mathbf{e}_z \times \langle \mathbf{H}\rangle + ..., \tag{18}$$

$$\text{where} \quad \widetilde{\boldsymbol{\mathcal{E}}} = \langle \mathbf{u}\times\mathbf{H}'\rangle. \tag{19}$$

Substituting (14), (16) and (18) into (2), we obtain the growth rate of the mean field for small j as

$$p \cong \pm|\alpha|j. \tag{20}$$

That is, the α-effect can explain the linear behaviour of $\mathrm{Re}[p]$ as a function of j around $j \sim 0$ in the dispersion relations (figure 4). In addition, (20) shows that one of the two branches is always a growing solution.

As j increases, the behaviours of $\mathrm{Re}[p]$ for $Rm \ll 1$ and for $Rm \gtrsim \mathrm{O}(1)$ become different. For $Rm = 8 \sim \mathrm{O}(1)$, the growth rate of the component with $j \sim 1/2$ increases above that expected under the α-effect approximation (18). In contrast, the growth rates for $Rm = 1/8 < 1$ do not exceed (20) for any j (figure 4). In particular, the growth rate of the component with wavenumber $j \sim 1/2$ for $Rm = 8$ is the fastest of the whole range of Rm. This feature is important since Rm in the Earth's core is estimated to be in the range 1–10^2. The nonlinear behaviour of $\mathrm{Re}[p]$ as a function of j for $j = \mathrm{O}(1)$ cannot be explained even if anisotropy is introduced in the expressions of α and β. In the following sections, we show that

the nonlocal and non-instantaneous effects of the electromotive force are essential in understanding the nonlinear behaviour of Roberts' dispersion relation for $Rm \gtrsim 1$.

3 Formulation of the kernel ϕ_{qr} for G.O. Roberts' flow

We now reduce the nonlocal and non-instantaneous kernel ϕ_{qr}, defined as (5), to a form appropriate for Roberts' problem. To achieve this, we change the formulation from an eigenvalue problem, a traditional form for the kinematic dynamo problem, to a time-evolution problem.

We apply a Fourier–Laplace transform to the problem. This transform is useful for understanding the relation between the time-evolution problem and the eigenvalue problem, since in the Fourier–Laplace transform functions of (z,t) are expanded in terms of $\exp(pt+\mathrm{i}jz)$, which is the form of the eigenfunctions (10) and (11) of the eigenvalue problem. The magnetic field $\mathbf{B}$, its horizontal average $\langle\mathbf{B}\rangle$ and its fluctuating part $\mathbf{B}'$ are expanded as

$$\mathbf{B}(x,y,z,t) = \frac{1}{2\pi}\frac{1}{2\pi\mathrm{i}}\int_{-\infty}^{\infty}\mathrm{d}j\int_{\nu-\mathrm{i}\infty}^{\nu+\mathrm{i}\infty}\mathrm{d}p\mathbf{H}(x,y,j,p)\exp\left(pt+\mathrm{i}jz\right), \tag{21}$$

$$\langle\mathbf{B}\rangle(z,t) = \frac{1}{2\pi}\frac{1}{2\pi\mathrm{i}}\int_{-\infty}^{\infty}\mathrm{d}j\int_{\nu-\mathrm{i}\infty}^{\nu+\mathrm{i}\infty}\mathrm{d}p\langle\mathbf{H}\rangle(j,p)\exp\left(pt+\mathrm{i}jz\right), \tag{22}$$

and

$$\mathbf{B}'(x,y,z,t) = \frac{1}{2\pi}\frac{1}{2\pi\mathrm{i}}\int_{-\infty}^{\infty}\mathrm{d}j\int_{\nu-\mathrm{i}\infty}^{\nu+\mathrm{i}\infty}\mathrm{d}p\mathbf{H}'(x,y,j,p)\exp\left(pt+\mathrm{i}jz\right), \tag{23}$$

respectively, where the horizontal average is defined by (12), and ν is a real number chosen so that the contour path of integration lies within the region of convergence of each Laplace-transformed function. Similarly, the Fourier–Laplace transform of the electromotive force $\boldsymbol{\mathcal{E}}$ is given by

$$\boldsymbol{\mathcal{E}}(z,t) = \frac{1}{2\pi}\frac{1}{2\pi\mathrm{i}}\int_{-\infty}^{\infty}\mathrm{d}j\int_{\nu-\mathrm{i}\infty}^{\nu+\mathrm{i}\infty}\mathrm{d}p\widetilde{\boldsymbol{\mathcal{E}}}(j,p)\exp\left(pt+\mathrm{i}jz\right), \tag{24}$$

where $\widetilde{\ }$ represents a Fourier–Laplace transformed function. Substituting (21), (22), (23) and (24) into the fluctuating part of the induction equation (4), we obtain

$$p\mathbf{H}' - \widetilde{\nabla}\times(\mathbf{u}\times\mathbf{H}') + \mathrm{i}\mathbf{j}\times\widetilde{\boldsymbol{\mathcal{E}}} - Rm^{-1}\widetilde{\nabla}^2\mathbf{H}' = \widetilde{\nabla}\times(\mathbf{u}\times\langle\mathbf{H}\rangle), \tag{25}$$

where $\widetilde{\nabla}$ is defined as

$$\widetilde{\nabla} = \left(\frac{\partial}{\partial x}, \frac{\partial}{\partial y}, \mathrm{i}j\right). \tag{26}$$

The fluctuating field $\mathbf{H}'$ is produced by the right-hand-side term $\widetilde{\nabla}\times(\mathbf{u}\times\langle\mathbf{H}\rangle)$. Hereafter, the forcing mean field $\langle\mathbf{H}\rangle$ or $\langle\mathbf{B}\rangle$ in the equation of the fluctuating field (25) or (4) is called the 'source field'. Equation (25) shows that $\mathbf{H}'$ is a linear functional of $\langle\mathbf{H}\rangle$ and is a function of j, p, x and y. The electromotive force $\widetilde{\boldsymbol{\mathcal{E}}}$ defined as (19) should therefore be proportional to $\langle\mathbf{H}\rangle$ and be a function of j and p. Thus the general form of $\widetilde{\boldsymbol{\mathcal{E}}}$ in (j,p) space can be expressed as

$$\widetilde{\mathcal{E}}_q(j,p) = \widetilde{\phi}_{qr}(j,p)\langle H\rangle_r(j,p) \quad (q,r=1,2,3), \tag{27}$$

where $\widetilde{\phi}_{qr}$ is a second-rank tensor and a complex function of j and p, and is determined by the flow $\mathbf{u}$. Moreover, symmetry about the $z = 0$ plane requires that $\widetilde{\mathcal{E}}_z = 0$. Since $\langle H_z \rangle = 0$ (15), (27) is essentially two-dimensional and may be written as

$$\begin{pmatrix} \widetilde{\mathcal{E}}_x \\ \widetilde{\mathcal{E}}_y \end{pmatrix} = \begin{pmatrix} \widetilde{\phi}_{xx}(j,p)\ \widetilde{\phi}_{xy}(j,p) \\ \widetilde{\phi}_{yx}(j,p)\ \widetilde{\phi}_{yy}(j,p) \end{pmatrix} \begin{pmatrix} \langle H_x \rangle \\ \langle H_y \rangle \end{pmatrix}, \tag{28}$$

which is a generalization of (18). The transformation of (28) into (z,t) space gives

$$\mathcal{E}_q(z,t) = \int_{-\infty}^{t} \int_{-\infty}^{\infty} \phi_{qr}(z - z', t - t') \langle B \rangle_r(z', t') \mathrm{d}z' \mathrm{d}t' \quad (q, r = 1, 2), \tag{29}$$

where

$$\phi_{qr}(z,t) = \frac{1}{2\pi} \frac{1}{2\pi \mathrm{i}} \int_{-\infty}^{\infty} \mathrm{d}j \int_{\nu - \mathrm{i}\infty}^{\nu + \mathrm{i}\infty} \mathrm{d}p \widetilde{\phi}_{qr}(j,p) \exp(pt + \mathrm{i}jz), \tag{30}$$

and its inverse transform is given by

$$\widetilde{\phi}_{qr}(j,p) = \int_{-\infty}^{\infty} \mathrm{d}z \int_{0}^{\infty} \mathrm{d}t \phi_{qr}(z,t) \exp(-pt - \mathrm{i}jz). \tag{31}$$

Equation (29) is the general form of the electromotive force in the two-dimensional problem and is a two-dimensional variant of (5). The function ϕ_{qr} includes nonlocal and non-instantaneous effects of the electromotive force, as opposed to α in (6), which expresses only local and instantaneous effects. The memory effect is expressed by the dependence of $\widetilde{\phi}_{qr}$ on p.

Symmetry can be used to reduce the number of independent components of the tensor $\widetilde{\phi}_{qr}$ (e.g. Rädler and Brandenburg 2003). Since $\mathbf{u}$ is invariant under 90° rotation around the z-axis together with a translation of π in the x or y direction, $\widetilde{\phi}_{qr}$ is axisymmetric around $\mathbf{e}_z$. The general form of an axisymmetric two-dimensional second-order tensor is given by

$$\begin{pmatrix} \widetilde{\phi}_{xx}(j,p)\ \widetilde{\phi}_{xy}(j,p) \\ \widetilde{\phi}_{yx}(j,p)\ \widetilde{\phi}_{yy}(j,p) \end{pmatrix} = \begin{pmatrix} c_1(j,p) & \mathrm{i}jc_2(j,p) \\ -\mathrm{i}jc_2(j,p) & c_1(j,p) \end{pmatrix}, \tag{32}$$

where c_1 and c_2 are arbitrary complex functions. The reality of ϕ_{qr} in (z,t) space requires $c_i^{\dagger}(j,p) = c_i(-j,p)$, where † represents the complex conjugate and $i = 1, 2$. Symmetry about the $z = 0$ plane leads to $c_i(j,p) = c_i(-j,p)$. Therefore c_1 and c_2 are pure real and independent of the sign of j. Thus (28) reduces to

$$\begin{pmatrix} \widetilde{\mathcal{E}}_x \\ \widetilde{\mathcal{E}}_y \end{pmatrix} = \begin{pmatrix} \widetilde{\varphi}(|j|,p) & \mathrm{i}j\widetilde{\psi}(|j|,p) \\ -\mathrm{i}j\widetilde{\psi}(|j|,p) & \widetilde{\varphi}(|j|,p) \end{pmatrix} \begin{pmatrix} \langle H_x \rangle \\ \langle H_y \rangle \end{pmatrix}, \tag{33}$$

where $\widetilde{\varphi}$ and $\widetilde{\psi}$ are real functions of j and p. The corresponding expression in (z,t) space is

$$\begin{aligned} \boldsymbol{\mathcal{E}}(z,t) = & \int_{-\infty}^{t} \int_{-\infty}^{\infty} \varphi(z - z', t - t') \langle \mathbf{B} \rangle(z', t') \mathrm{d}z' \mathrm{d}t' \\ & - \mathbf{e}_z \times \frac{\partial}{\partial z} \int_{-\infty}^{t} \int_{-\infty}^{\infty} \psi(z - z', t - t') \langle \mathbf{B} \rangle(z', t') \mathrm{d}z' \mathrm{d}t', \end{aligned} \tag{34}$$

where φ and ψ are the inverse Fourier–Laplace transforms of $\widetilde{\varphi}$ and $\widetilde{\psi}$, respectively. These equations show that the behaviour of the electromotive force in Roberts' problem can sufficiently be described by only two functions, φ and ψ.

The dispersion relation of the mean field can readily be written in terms of $\widetilde{\varphi}$ and $\widetilde{\psi}$ as follows. Substituting (33) into the equation of the mean field (2) in (j,p) space, we have

$$p^* \begin{pmatrix} \langle H_x \rangle(j,p) \\ \langle H_y \rangle(j,p) \end{pmatrix} = \mathrm{i}j \begin{pmatrix} \mathrm{i}j\widetilde{\psi}(|j|,p) & -\widetilde{\varphi}(|j|,p) \\ \widetilde{\varphi}(|j|,p) & \mathrm{i}j\widetilde{\psi}(|j|,p) \end{pmatrix} \begin{pmatrix} \langle H_x \rangle(j,p) \\ \langle H_y \rangle(j,p) \end{pmatrix}, \tag{35}$$

where

$$p^* = p + Rm^{-1}j^2. \tag{36}$$

Solving the eigenvalue problem (35), we obtain the dispersion relation:

$$p^*_{1,2} = \pm\widetilde{\varphi}(|j|,p)j - \widetilde{\psi}(|j|,p)j^2. \tag{37}$$

Both growing and decaying solutions always exist for sufficiently small j regardless of the sign of $\widetilde{\varphi}$ unless $\widetilde{\varphi}(0,p) = 0$. The growing branch of the dispersion relation is written as

$$p^* = |\widetilde{\varphi}(|j|,p)|\, j - \widetilde{\psi}(|j|,p)j^2. \tag{38}$$

The diagonal component $\widetilde{\varphi}$ functions to intensify the mean field. The growth rate p increases as the absolute value of $\widetilde{\varphi}$ increases. The non-diagonal component $\widetilde{\psi}$ functions to decrease the mean field if it is positive (eddy diffusion) and to increase the mean field if it is negative. Note that (37) basically represents two eigenvalues, whereas the original kinematic dynamo problem has an infinite number of eigenvalues. This results from the neglect of the 'small-scale dynamo' mentioned in the Introduction.

The relationship between the dispersion relation $p = p(j)$ and the kernel $\widetilde{\varphi}(j,p)$ can be illustrated on the (j,p) plane as follows, if $\widetilde{\psi}$ is constant. Equation (37) may be understood as being the solution of the simultaneous equations

$$\widetilde{\varphi} = \pm\widetilde{\varphi}(j,p) \tag{39}$$

and

$$\widetilde{\varphi} = (p^* + \widetilde{\psi}j^2)/j. \tag{40}$$

Therefore, the intersection of the two topographies described by the two equations above gives the dispersion relation on the (j,p) plane. This relation can serve as a guide to identifying features of $\widetilde{\varphi}(j,p)$ which are important to the behaviour of the dispersion relation.

Step responses $\Phi(z,t)$ and $\Psi(z,t)$ defined as

$$\begin{aligned} \Phi(z,t) &\equiv \int_0^t \varphi(z,t')\mathrm{d}t', \\ \Psi(z,t) &\equiv \int_0^t \psi(z,t')\mathrm{d}t' \end{aligned} \tag{41}$$

are used in the following to display the response kernel ϕ_{qr} in (z,t) space, in addition to $\widetilde{\varphi}(j,p)$ and $\widetilde{\psi}(j,p)$ in (j,p) space. They are the responses to a source field given by the form of the step function

$$\langle \mathbf{B} \rangle = \langle \mathbf{B}_0 \rangle \delta(z)\Theta(t), \tag{42}$$

where $\langle \mathbf{B}_0 \rangle$ is the strength of the source field, $\delta(z)$ is the delta function and $\Theta(t)$ is the step function, given by

$$\Theta(t) = \begin{cases} 1 & \text{for} \quad 0 \le t' \le t, \\ 0 & \text{for} \quad t < t' < \infty. \end{cases} \tag{43}$$

For the source field above, the electromotive force becomes

$$\begin{aligned} \mathcal{E}_q(z,t) &= \int_{-\infty}^{t} \mathrm{d}t' \int_{-\infty}^{\infty} \mathrm{d}z' \phi_{qr}(z-z', t-t') \langle B_0 \rangle_r \Theta(t') \delta(z') \\ &= \Phi(z,t) \langle B_0 \rangle_q - \frac{\partial \Psi(z,t)}{\partial z} \varepsilon_{qrs} e_r \langle B_0 \rangle_s. \end{aligned} \tag{44}$$

Equation (44) represents how the responses Φ and Ψ operate if the source field $\langle \mathbf{B} \rangle$ is applied suddenly at $t = 0$ on the $|z| = 0$ surface and is maintained for $t > 0$.

The responses Φ and Ψ in (z,t) space have simple approximate relations with $\widetilde{\varphi}$ and $\widetilde{\psi}$ in (j,p) space. The Laplace transformation between the time t domain and the growth rate p domain can be approximated as

$$\begin{aligned} \widetilde{\varphi}(j,p) &= \int_{-\infty}^{\infty} \mathrm{d}z \int_{0}^{\infty} \mathrm{d}t \; \varphi(z,t) \mathrm{e}^{-pt - \mathrm{i}jz} \\ &\sim \int_{-\infty}^{\infty} \mathrm{d}z \int_{0}^{1/p} \mathrm{d}t \; \varphi(z,t) \mathrm{e}^{-\mathrm{i}jz} = \int_{-\infty}^{\infty} \Phi(z, t = 1/p) \mathrm{e}^{-\mathrm{i}jz} \mathrm{d}z. \end{aligned} \tag{45}$$

In the same way, $\widetilde{\psi}(j,p)$ and $\Psi(z,t)$ are approximately related as

$$\widetilde{\psi}(j,p) \sim \int_{0}^{\infty} \Psi(z, t = 1/p) \mathrm{e}^{-\mathrm{i}jz} \mathrm{d}z. \tag{46}$$

Hence, we can regard $\widetilde{\varphi}$ and $\widetilde{\psi}$ at $p = 1/t (> 0)$ in (j,p) space as the Fourier transforms of Φ and Ψ at the time t.

The traditional α and β are related to $\widetilde{\varphi}$ and $\widetilde{\psi}$, or the spatial integrals of Φ and Ψ, as follows. The traditional α may be defined as the coefficient of proportionality between the electromotive force and the mean field $\langle \mathbf{B} \rangle$, which is uniform in time and space. When the source field $\langle \mathbf{B} \rangle$ is constant, the electromotive force (34) becomes

$$\boldsymbol{\mathcal{E}}(z,t) = \langle \mathbf{B} \rangle \int_{-\infty}^{t} \mathrm{d}t' \int_{-\infty}^{\infty} \mathrm{d}z' \varphi(z-z', t-t'). \tag{47}$$

Consequently, the traditional α is

$$\alpha = \int_{-\infty}^{t} \mathrm{d}t' \int_{-\infty}^{\infty} \mathrm{d}z' \varphi(z-z', t-t') = \int_{-\infty}^{\infty} \Phi(z, t \to \infty) \mathrm{d}z. \tag{48}$$

In this way α is a spatial integral of Φ in the long-time limit. From (48) and (45), α is connected with $\widetilde{\varphi}$ as

$$\alpha = \widetilde{\varphi}(j = 0, p = 0). \tag{49}$$

Furthermore, when the source field is proportional to z, $\langle \mathbf{B} \rangle(z) = Az\mathbf{e}_x$ with a constant A, the electromotive

force (34) reduces to

$$\boldsymbol{\mathcal{E}}(z,t) = Az\mathbf{e}_x \int_{-\infty}^{t}\int_{-\infty}^{\infty} \varphi(z-z',t-t')\mathrm{d}z'\mathrm{d}t' - A\mathbf{e}_y \int_{-\infty}^{t}\int_{-\infty}^{\infty} \psi(z-z',t-t')\mathrm{d}z'\mathrm{d}t'. \tag{50}$$

On the other hand, substituting $\langle \mathbf{B}\rangle(z) = Az\mathbf{e}_z$ into the definition of β in (8), we get $\mathcal{E}_y = -\beta A$. Comparing this expression with the y-component of (50), we obtain

$$\beta = \int_{-\infty}^{\infty} \Psi(z, t\to\infty)\mathrm{d}z. \tag{51}$$

Thus β is a spatial integral of Ψ, in a way similar to α. From (51) and (46), its relations with $\widetilde{\psi}$ is written as

$$\beta = \widetilde{\psi}(j=0, p=0). \tag{52}$$

To summarize, the two sets of functions $\{\Phi(z,t), \Psi(z,t)\}$ and $\{\widetilde{\varphi}(j,p), \widetilde{\psi}(j,p)\}$ have their own natural advantages. The set $\{\Phi(z,t), \Psi(z,t)\}$ is suitable for showing short-term and short-range responses. The set $\{\widetilde{\varphi}(j,p), \widetilde{\psi}(j,p)\}$ is suitable for showing long-term and long-range responses. The former set is easier to understand intuitively because it is a set of functions in physical space, whereas the latter set is useful for understanding the connection between the electromotive force and the dispersion relation because they are related by (38).

4 Results: characteristics of the mean electromotive force $\boldsymbol{\phi_{qr}}$

In this section, we show the numerical results of the responses $\widetilde{\varphi}, \widetilde{\psi}, \Phi$ and Ψ caused by Roberts' flow (9) and explain their characteristics. The numerical method is explained in Appendix A. The range of the magnetic Reynolds number in our calculations is $1/64 \le Rm \le 10$. We do not carry out calculations for $Rm > 10$, since developing the boundary layer in three-dimensional space with thickness $\delta_\mathrm{b} \sim \mathrm{O}(Rm^{-1/2})$ requires considerable computation time.

We first calculate the traditional α defined by (48) and (49) to see the overall behaviour of the electromagnetic induction as a function of the magnetic Reynolds number Rm. Numerical results are shown in figure 5, together with asymptotic behaviours reported in past studies. For $Rm \ll 1$, the first-order smoothing approximation(G.O.Roberts 1972, Rädler *et al.* 2002) gives

$$\alpha \sim -Rm, \tag{53}$$

as we shall see in section 4.1. For $Rm \to \infty$, the boundary layer theory based on flux explusion(Childress 1979, Anufriyev and Fishman 1982, Soward 1987) gives

$$\alpha \sim -0.5327(2/Rm)^{1/2}. \tag{54}$$

Our numerical results reproduce these asymptotes very well. Furthermore, we can identify three regions based on the applicability of these approximations. For $Rm \lesssim 1/4$ (Region 1) the first-order smoothing approximation holds and for $Rm \gtrsim 4$ (Region 3) the boundary layer theory holds. The interval $1/4 \lesssim Rm \lesssim 4$ (Region 2) is the transition between these two regions. As we shall see in section 4.2, non-localness and non-instantaneousness increase with Rm in Region 2. In the following three subsections, we explain the responses $\widetilde{\varphi}, \widetilde{\psi}, \Phi$ and Ψ for $Rm = 1/32$ (Region 1), $Rm = 1/4, 1$ and 4 (Region 2) and $Rm = 8$ (Region 3).

4.1 *Region 1: Rm* $\lesssim 1/4$

In this section, we confirm that φ and ψ reduce to the traditional α- and β-effects for $Rm \lesssim 1/4$.

Figure 6a shows the contour of the time development of the response Φ forced by the source field (42) for $Rm = 1/32$. A negative Φ is established almost instantaneously at $t = 0$ and becomes steady after $t \sim Rm$, which is the diffusion time in our non-dimensionalisation. The negative Φ is concentrated near the source field at $|z| \sim 0$. The response Ψ behaves similarly. A steady positive Ψ concentrated near $|z| = 0$ is established almost instantaneously within $t \lesssim Rm$ (figure 6b). Thus Φ and Ψ show instantaneous and local responses if Rm is small enough.

Figure 7 shows the contours of $\widetilde{\varphi}$ and $\widetilde{\psi}$ in (j, p) space for the same Rm. These contours correspond to figure 6 through the relations (45) and (46). The response $\widetilde{\varphi}(j, p)$ depends only slightly on $\mathrm{Re}[p]$ and depends weakly on j. The very weak dependence of $\widetilde{\varphi}(j, p)$ on p means that the response is instantaneous. The weak dependence on j means that the response is local. The dependence on j is due to the magnetic diffusion effect, as described below. The response $\widetilde{\psi}$ shows a similar behaviour (figure 7b). Thus $\widetilde{\varphi}$ and $\widetilde{\psi}$ in (j, p) space demonstrate that $\varphi(z, t)$ and $\psi(z, t)$ are local and instantaneous for $Rm \lesssim 1/4$, which is consistent with the results for Φ and Ψ in (z, t) space (figure 6).

The analytical solutions of φ and ψ can easily be obtained for $Rm \ll 1$. We first consider which terms contribute most to the balance in (25). When $Rm \ll 1$ and $j = \mathrm{O}(1)$, we have

$$\mathbf{H}' \sim Rm\langle \mathbf{H} \rangle \tag{55}$$

in order that the left-hand-side balances the right-hand-side source term. If we further assume that

$$p = \mathrm{O}(Rm^{-1}), \tag{56}$$

the equation of the fluctuating part (25) becomes

$$\left(p - Rm^{-1}\widetilde{\nabla}^2\right)\mathbf{H}' = -\widetilde{\nabla} \times (\mathbf{u} \times \langle \mathbf{H} \rangle). \tag{57}$$

The solution of (57) is obtained as

$$\mathbf{H}' = \frac{1}{p^* + Rm^{-1}} \begin{pmatrix} -\mathrm{i}j(\cos x - \cos y) & \cos y \\ \cos x & -\mathrm{i}j(\cos x - \cos y) \\ -\sin x & \sin y \end{pmatrix} \begin{pmatrix} \langle H_x \rangle \\ \langle H_y \rangle \end{pmatrix}, \tag{58}$$

as shown in Appendix B. Taking the cross product with the flow $\mathbf{u} \times \mathbf{H}'$ and averaging it, we obtain the electromotive force

$$\widetilde{\boldsymbol{\mathcal{E}}} = \langle \mathbf{u} \times \mathbf{H}' \rangle = \frac{1}{p^* + Rm^{-1}} \begin{pmatrix} -1 & \mathrm{i}j \\ -\mathrm{i}j & -1 \\ 0 & 0 \end{pmatrix} \begin{pmatrix} \langle H_x \rangle \\ \langle H_y \rangle \end{pmatrix}. \tag{59}$$

Thus $\widetilde{\varphi}$ and $\widetilde{\psi}$ in (j, p) space become

$$\widetilde{\varphi}(j, p^*) = -\widetilde{\psi}(j, p^*) = -\frac{1}{p^* + Rm^{-1}}, \tag{60}$$

which are transformed into φ and ψ in (z,t) space according to (30) as

$$\varphi(z,t) = -\psi(z,t) = -\frac{1}{2\pi}\int_{-\infty}^{\infty} \mathrm{e}^{-Rm^{-1}(1+j^2)t}\mathrm{e}^{\mathrm{i}jz}\mathrm{d}j \tag{61}$$

$$= -\frac{1}{2\pi}\sqrt{\frac{\pi}{Rm^{-1}t}}\exp\left[-Rm^{-1}t - \frac{z^2}{4Rm^{-1}t}\right]. \tag{62}$$

Here we have used an integral formula

$$\int_{s_\mathrm{r}-\mathrm{i}\infty}^{s_\mathrm{r}+\mathrm{i}\infty} \frac{1}{A+s}\mathrm{e}^{st}\mathrm{d}s = 2\pi\ \mathrm{i}\ \mathrm{e}^{-At} \tag{63}$$

where s is complex, $s = s_\mathrm{r} + \mathrm{i}s_\mathrm{i}$, and A is a constant. When $t \sim 2Rm$, or twice the diffusion time, the responses φ and ψ almost vanish and the integrated responses Φ and Ψ approach a steady state within 10%. Integrating (62) gives the steady state of Φ and Ψ as

$$\Phi(z, t\to\infty) = -\Psi(z, t\to\infty) = -\frac{1}{2}Rm\ \mathrm{e}^{-|z|}, \tag{64}$$

where we have used another integral formula

$$\int_0^\infty \frac{1}{\sqrt{x}}\mathrm{e}^{-ax-b^2/x}\mathrm{d}x = \sqrt{\frac{\pi}{a}}\mathrm{e}^{-2b\sqrt{a}} \quad (a,b>0) \tag{65}$$

where a and b are positive constants. This analytical result (64) reproduces the numerical result very well, as shown in figure 8. To summarize, the analytical results confirm and clarify the local and instantaneous nature of φ and ψ for $Rm \ll 1$.

The traditional α and β are obtained by the two methods explained in section 3. We can derive them from Φ and Ψ in (z,t) space by substituting (64) into (48) and (51) as

$$\begin{aligned}\alpha &= \int_{-\infty}^{\infty}\Phi(\xi, t\to\infty)\mathrm{d}\xi = -Rm,\\ \beta &= \int_{-\infty}^{\infty}\Psi(\xi, t\to\infty)\mathrm{d}\xi = Rm.\end{aligned} \tag{66}$$

The same result may be obtained by substituting (60) into (49) and (52) as

$$\alpha = \widetilde{\varphi}(0,0) = -Rm, \tag{67}$$

$$\beta = \widetilde{\psi}(0,0) = Rm. \tag{68}$$

Since the responses $\widetilde{\varphi}$ and $\widetilde{\psi}$ for $p \ll Rm^{-1}$ ($t \gg Rm$) and $j \ll 1$ reduce to

$$\widetilde{\varphi} = -\widetilde{\psi} = -Rm, \tag{69}$$

the traditional α and β are valid for $p \ll Rm^{-1}$ and $j \ll 1$.

4.2 *Region 2 (transition):* $1/4 \lesssim Rm \lesssim 4$

Figures 9 and 10 show the responses in the transition region $1/4 \lesssim Rm \lesssim 4$. Figure 9 shows $\{\Phi, \Psi\}$ for $Rm = 1/4, 1$ and 4 in (z,t) space and figure 10 shows $\{\widetilde{\varphi}, \widetilde{\psi}\}$ for the same magnetic Reynolds numbers in

(j,p) space. The kernels $\{\Phi,\Psi\}$ and $\{\widetilde{\varphi},\widetilde{\psi}\}$ become increasingly nonlocal and non-instantaneous as Rm increases.

Figures 9 i)a and ii)a show the kernel Φ for $Rm=1/4$ and 1, respectively. The similarity to figure 6a ($Rm \ll 1/4$) indicates that localness and instantaneousness still apply. However, Φ already deviates from (64) and the deviation increases with Rm. The steady state magnitude of ΦRm^{-1} at $z=0$ should be $1/2$ if (64) is valid, but it is 0.48 and 0.36 for $Rm=1/4$ and 1, respectively. For $Rm=1$, the time taken to reach the steady state is a little shorter than (64) predicts; $\Phi(z=0,t)$ is already within 10% of the steady state value at $tRm^{-1}=1$, i.e. the diffusion time. The spatial structure of the function $\Phi(z,t\to\infty)$ is almost $\mathrm{e}^{-|z|}$ for $Rm=1/4$ and 1.

For $Rm=4$, non-instantaneousness and nonlocalness are apparent. Figure 9 iii)a shows that a negative Φ is generated initially around $|z|=0$ and spreads with time in the z direction until $t\sim 2$. After that, the spread stops and Φ increases until $t\sim 4$. The sign of the response even turns positive at $t\sim 4$ over $\pi \lesssim |z| \lesssim 4\pi$. A weak oscillation follows, becoming steady at $tRm^{-1}\sim 4$, which is slower than (62) predicts. Its amplitude in the steady state is $|\Phi(z=0,t\to\infty)Rm^{-1}|\sim 0.12$, much smaller than (64) predicts.

The kernels $\widetilde{\varphi}$ in (j,p) space display corresponding features in accordance with (45) (figure 10 a). The magnitude of the kernel $|\widetilde{\varphi}Rm^{-1}|$ at $j=p=0$ should be unity if (60) is valid, but it is 0.97 and 0.75 for $Rm=1/4$ and 1, respectively. Non-instantaneousness and nonlocalness are apparent for $Rm=4$ (figure 10 iii)a) as a non-monotonic dependence of $\widetilde{\varphi}(j,p)$ on j and p. In particular, two notable features appear in the region $0\lesssim j\lesssim 1$ and $-0.5\lesssim p\lesssim 0$: a valley extending from $(j,p)\sim(0.5,0)$ to $(j,p)\sim(1,-0.5)$ and a singular ring near $(j,p)\sim(1/2,-2/5)$.

The off-diagonal response $\Psi(z,t)$ also becomes increasingly non-instantaneous and nonlocal with Rm (figure 9b). The deviation from (64) increases with Rm and the relation $\Phi=-\Psi$ is no longer valid. The steady state response $|\Psi Rm^{-1}|$ at $z=0$ should be $1/2$ according to (64), but it is 0.47 for $Rm=1/4$ and 0.33 for $Rm=1$. For $Rm=1/4$ (figure 9 i)b), the spatial form of Ψ remains nearly $\mathrm{e}^{-|z|}$, but it changes sign at $|z|\sim(5/2)\pi$. For $Rm=1$ (figure 9 ii)b), the deviation from the relation $\Phi=-\Psi$ becomes apparent. The response Ψ slightly overspreads in the z direction at $tRm^{-1}\sim 1$ and approaches a steady state at $tRm^{-1}\sim 4$. The steady response changes sign at $|z|\sim(3/4)\pi$, closer to the source field than for $Rm=1/4$. For $Rm\sim 4$ (figure 9 iii)b), non-instantaneousness and nonlocalness are clear. A positive response Ψ is generated initially around $|z|=0$ and spreads in the z direction with time until $t\sim 1$. After that, it decreases until a negative region centered at $|z|\sim\pi/2$ spreads and becomes maximum at $t\sim 4$. The negative region shrinks again to zero at $t\sim 7$ and an oscillatory behaviour follows until it becomes steady at $t\sim 22$.

The behaviour of the kernel $\widetilde{\psi}$ in (j,p) space reflects that of Ψ in accordance with (46). The magnitude of $\widetilde{\psi}$ becomes smaller than (60) predicts. While $|\widetilde{\psi}(0,0)Rm^{-1}|$ should be unity if (60) held, it is 0.94 for $Rm=1/4$. Equation (60) is a monotonically decreasing function of j and p. However, $\widetilde{\psi}$ for $Rm=1$ is not monotonic (figure 10 ii)b) and has a small hill extending from $(j,p)\sim(0,1/4)$ to $(j,p)\sim(3/4,-1/2)$. The hill passes through $(j,p)\sim(1/2,0)$, which corresponds to a smooth wavy structure with a wavelength $\sim 4\pi$ of a steady state of $\Psi(z,t)$ (figure 9 ii)b). For $Rm=4$ (figure 10 iii)b), the kernel $\widetilde{\psi}$ has a negative valley which runs from $(j,p)\sim(1/2,1/4)$ to $(j,p)\sim(1,-1/2)$ and a singular ring centered at $(j,p)\sim(1/2,-2/5)$. The valley corresponds to a negative Ψ at $t\sim 4$ according to (46).

4.3 *Region 3: Rm* $\gtrsim$ 4

The response Φ for $Rm\gtrsim 4$ exhibits non-instantaneous and nonlocal behaviour. Figure 11a shows the response Φ for $Rm=8$. After the source field is applied at $t=0$, a negative Φ is first produced near the source field at $|z|=0$ and spreads out in the z direction until $t\sim 2$. Then Φ begins to increase, becomes positive at $t\sim 4$ over the interval $\pi/2\lesssim|z|\lesssim 4\pi$ and becomes maximum at $t\sim 6$ and $|z|\sim\pi$. It then approaches a steady state in an oscillatory manner. Apart from the oscillatory part, a boundary layer, in which Φ is negative, forms around $|z|=0$. This boundary layer represents a local and instantaneous part of the electromotive force.

Figure 12a shows $\widetilde{\varphi}$ in (j,p) space for $Rm=8$. Equation (45) can serve as a guide to examine the

correspondence between Φ and the positive-p part of $\widetilde{\varphi}$. For $p \gtrsim 0.5$, $\widetilde{\varphi}$ for $Rm = 4$ and $Rm = 8$ behave similarly. In accordance with (45), Φ for $Rm = 4$ and $Rm = 8$ look similar at $t \lesssim 2$. This similarity means that the initial evolution of the electromotive force is entirely due to advection and is unaffected by diffusion. Subsequently, diffusion begins to operate, resulting in a difference between $Rm = 4$ and $Rm = 8$. Of particular importance for the dispersion relation is the valley running from $(j, p) \sim (1/2, 1/6)$ to $(j, p) \sim (3/2, -1/2)$ for $Rm = 8$. Its relation to the dispersion relation will be discussed in the next section. This valley results in a wavy structure in (z, t) space with wavenumber $j \sim 1/2$ at $t \gtrsim 4$ (figure 11a). The negative-p part of $\widetilde{\varphi}$ is difficult to interpret. Many singularities exist, one of which is apparent in figure 12a around $(j, p) \sim (1/2, -1/6)$ and has a circular structure on the (j, p) plane. The nature of these singularities is yet to be examined.

Figure 13a shows $\widetilde{\varphi}$ for three values of p as functions of j. For $p = 2.0$, the $|\widetilde{\varphi}|$ decreases monotonically with j and is smooth. For $p \lesssim 0.3$, the dependence of $|\widetilde{\varphi}|$ on j becomes non-monotonic. For $p \sim 1/6$, $|\widetilde{\varphi}|$ shows a peak at $j \sim 1/2$, which is reflected in the wavy structure of Φ with a wavelength of about 4π at $t \sim 6$ in figure 11a.

The off-diagonal responses Ψ and $\widetilde{\psi}$ similarly show nonlocal and non-instantaneous behaviour. Figure 11b and figure 12b show $\Psi(z, t)$ in (z, t) space and $\widetilde{\psi}(j, p)$ in (j, p) space, respectively, for $Rm = 8$. A positive Ψ appears and spreads during $0 \lesssim t \lesssim 2$, corresponding to a broad positive region of $\widetilde{\psi}$ for $p \gtrsim 0.5$, in accordance with (46). The response $\Psi(z, t)$ turns negative at $t \sim 2$ over $0 \lesssim |z| \lesssim 2\pi$ and oscillatory behaviour follows with a period of about 8. A negative Ψ implies negative diffusion, which can enhance the dynamo action. Negative values appear also in $\widetilde{\psi}$ for $j \lesssim 1$ and $0 \lesssim p \lesssim 0.5$. It is notable that $\widetilde{\psi}$ vanishes near the peak in the dispersion curve at $j \sim 1/2$. According to (46), this corresponds to a vanishing Ψ at $t \sim 6$.

Figure 13b shows the function $\widetilde{\psi}(j, p)$ at three values of p. For $p = 2.0$, $\widetilde{\psi}$ decreases monotonically with j and is positive at all j. For $p \lesssim 0.5$, $\widetilde{\psi}$ is negative, indicative of negative diffusion. At $p = 0.16 \sim 1/6$, the response $\widetilde{\psi}$ has a negative peak at $j \sim 1/2$, where $\widetilde{\varphi}$ also has a peak.

Calculations of the extended α-effect in previous works (Soward 1987, 1989, Plunian and Rädler 2002b) have represented only a part of the kernel ϕ_{qr}. Since both Soward (1987, 1989) and Plunian and Rädler (2002b) were interested in the dispersion relation, they focused on the extended α on the dispersion curve, which is a curve on the (j, p) plane. In contrast, our interest is in the general properties of the kernel ϕ_{qr}, in (5), not merely on the dispersion relation. Thus we aim to examine the behaviour of ϕ_{qr} or the generalized α on the whole (j, p) plane. In fact, taking $\widetilde{\varphi}$ and $\widetilde{\psi}$ in the dispersion relation in accord with the definition of Plunian and Rädler (2002b) (figure 14), we obtain a result identical with figure 3 in their paper.

5 Dispersion relation induced by ϕ_{qr}

In this section, we interpret the dispersion relation of Roberts' kinematic dynamo in terms of the approximate $\widetilde{\varphi}$ and $\widetilde{\psi}$ obtained in section 4. In section 5.1, we give an explicit expression of the dispersion relation for $Rm \ll 1$. In section 5.2, we semi-quantitatively describe the mechanism of the enhanced growth of the mean field for $Rm \gtrsim 4$ with a nonlocal and non-instantaneous electromotive force. Finally, section 5.3 presents an intuitive explanation of the generation of the nonlocal and non-instantaneous effects in relation to the twist of the magnetic lines of force.

5.1 *Dispersion relation of the mean field in terms of $\widetilde{\varphi}$ and $\widetilde{\psi}$: $Rm \ll 1$*

The analytical form of the response (60) can be used to explain the behaviour of the dispersion relation of the growing solution for $Rm \ll 1$. Substituting (60) into (37), we obtain four eigenvalues:

$$p^*_{1,2,3,4} = -\frac{1}{2Rm} \pm \frac{1}{2Rm}\sqrt{1 - 4Rm^2(j^2 \pm j)}. \tag{70}$$

Since $Rm \ll 1$, (70) can be expanded as

$$p_1^* = \quad +Rm\, j - Rm\, j^2 + \mathrm{O}\left(Rm^3(j^2-j)^2\right), \tag{71}$$

$$p_2^* = -\frac{1}{Rm} - Rm\, j + Rm\, j^2 - \mathrm{O}\left(Rm^3(j^2-j)^2\right), \tag{72}$$

if $4Rm^2|j^2-j| \ll 1$ and as

$$p_3^* = \quad -Rm\, j - Rm\, j^2 + \mathrm{O}\left(Rm^3(j^2+j)^2\right), \tag{73}$$

$$p_4^* = -\frac{1}{Rm} + Rm\, j + Rm\, j^2 - \mathrm{O}\left(Rm^3(j^2+j)^2\right), \tag{74}$$

if $4Rm^2(j+j^2) \ll 1$. The two branches p_1^* and p_3^* represent the growing and decaying solutions, respectively, of the α^2-dynamo with traditional α- and β-effects. The other two branches represented by p_2^* and p_4^* decay very rapidly. However, they are spurious because for these solutions $\mathbf{H}' \sim Rm^{-1}\langle\mathbf{H}\rangle$, which violates the assumption (55) needed in deriving these results. Hence, (71) and (73) are good approximations of the dispersion relation for $Rm \ll 1$ (figure 15a), while (72) and (74) are not (figure 15b). Thus the appropriate dispersion relation of the growing solution is represented by p_1^* (71), or

$$p^* = -\frac{1}{2Rm} + \frac{1}{2Rm}\sqrt{1+4Rm^2(j-j^2)}. \tag{75}$$

The mean-field generation described above is schematically illustrated in figure 16a. For simplicity, we focus on the α-effect and neglect the β-effect. Suppose that an initial mean field $\langle\mathbf{B}_0\rangle$ of the form (42) is placed at $z = 0$. It instantaneously generates a negative α-effect (62) near the given field $\langle\mathbf{B}_0\rangle$. The α-effect is localized, as is evident in figure 6. Then the α_1 induces a new field $\langle\mathbf{B}_1\rangle$ through the process described by (35). This field in turn generates α_2 around $\langle\mathbf{B}_1\rangle$ and gives rise to $\langle\mathbf{B}_2\rangle$. In this way, a helical mean magnetic field that grows with time is produced. This is the α^2-dynamo mechanism whose dispersion relation is expressed as (71) or (75).

5.2 *Dispersion relation of the mean field in terms of $\widetilde{\varphi}$ and $\widetilde{\psi}$: $Rm \gtrsim 4$*

We next consider the relation between the dispersion curve for $Rm \gtrsim 4$ and the nonlocal and non-instantaneous features of $\widetilde{\varphi}$ and $\widetilde{\psi}$.

The behaviour of $\widetilde{\varphi}(j,p)$ in the neighborhood of the dispersion curve is important for understanding the dispersion relation. The dispersion curve is the intersection between the contours of $\widetilde{\varphi}$ and the equation of the mean field (40), as explained in section 3. We have already noted in section 4.3 that the response of $\widetilde{\varphi}(j,p)$ has a valley that runs through $p \sim 1/6$ and $j \sim 1/2$, where the dispersion curve shows a peak. This indicates that the enhancement of the mean-field generation is caused by the valley of $\widetilde{\varphi}$.

In order to make the explanation above semi-quantitative, we approximate $\widetilde{\varphi}$ for $Rm = 8$ around $0 \lesssim p \lesssim 0.5$ and $0 \lesssim j \lesssim 1$ by

$$\widetilde{\varphi}(j,p) = -\varphi_0 - \frac{\varphi_1}{1+\left(\dfrac{j}{j_1}\right)^2} - \frac{\varphi_2}{1+\left(\dfrac{p-p_0+q_0j^2}{p_2}\right)^2}, \tag{76}$$

where $\varphi_0 = 0.065, \varphi_1 = 0.234, j_1 = 1.23, \varphi_2 = 0.11, q_0 = 0.38, p_0 = 0.33$ and $p_2 = 0.18$ (figure 17). The first and second terms on the right-hand side express a smooth feature which represents the instantaneous α-effect with spatial decay. The third term expresses the valley, which reflects a nonlocal memory effect. Substituting (76) into (38), we obtain an approximate dispersion relation of the generated mean field, shown as the dashed curve in figure 18. In calculating this curve, we assume $\widetilde{\psi} = 0$ for simplicity, because

$\widetilde{\psi}$ is small around $(j,p) \sim (1/2, 1/6)$. As figure 18 shows, the nonlocal and non-instantaneous feature of $\widetilde{\varphi}$ results in a growth rate which exceeds that produced only by the local and instantaneous α-effect.

The mechanism above is schematically illustrated in (z,t) space in figure 16b. For simplicity, as in figure 16a, we focus on the α-effect or the effect of φ and neglect the β-effect or the effect of ψ. As before, we suppose that an initial field $\langle \mathbf{B}_0 \rangle$ is placed at $z = 0$. In addition to a negative α_1 around $\langle \mathbf{B}_0 \rangle$, a positive nonlocal effect Φ_1 arises around $|z| \sim 2\pi$ far from the initial field $\langle \mathbf{B}_0 \rangle$, as shown in figure 11a. This nonlocal effect enhances the growth of a mean field with wavenumber $j \sim 1/2$ by augmenting the growth of the field $\langle \mathbf{B}_1 \rangle$ at $z \sim \pi$ generated by the local α_1 accompanying $\langle \mathbf{B}_0 \rangle$. As noted in section 4.3, the nonlocal effect results from the valley of $\widetilde{\varphi}(j,p)$ around $j \sim 1/2$.

5.3 *Relation between the electromotive force and magnetic lines of force*

Magnetic lines of force provide an intuitive explanation of the generation mechanism of ϕ_{qr}. Since magnetic lines of force are often used to interpret the results of magnetohydrodynamic numerical simulations, visualising the magnetic memory effect in terms of field lines provides further insight for interpreting numerical results.

Figure 19 shows the time evolution of typical magnetic lines of force for $Rm = 8$. It is calculated using (1) with an initial magnetic field of $\mathbf{B}(t=0) = (1,1,0)\delta(z)$. This is a situation similar to that for calculating Φ and Ψ. However (1) is used instead of (25) because magnetic lines of force cannot be divided into a mean and a deviation. This brings about an important difference. When calculating the kernels Φ and Ψ using (25), the mean field $\langle \mathbf{B} \rangle$ is independent of time. On the other hand, when calculating the magnetic lines of force using (1), the mean field $\langle \mathbf{B} \rangle$ changes with time.

The field lines evolve as follows. At $t \sim 0.5$, they undulate in the z direction and are twisted by at most about $\pm$ 20 degrees in the (x,y) plane (figure 19 i)a and c), forming a screw-like structure (figure 19 i)a and b). These screw-like field lines give rise to the local and instantaneous α-effect. At $t \sim 2$, the twist increases up to $\pm$ 90 degrees in the (x,y) plane (figure 19 ii)a and c), and the radius of the screw-loop increases to about π (figure 19 ii)a and b). At this point, the spread of negative Φ becomes maximum (figure 11 (a)). At the same time, the field lines become concentrated to form boundary layers near cell boundaries of the flow field (figure 19 ii)a and c). After this, field lines pass through convection cells which do not form a line. A loop of a magnetic line of force is not confined within a convection cell, as illustrated in figure 1, but meanders among different cells. At $t = 6.5$, field lines elongated in the z direction by more than π form loops in a direction opposite to the loops around $z \sim 0$ (figure 19 iii)b). The loop at $z \sim 2\pi$ is located at $(x,y) \sim (2\pi, 5\pi)$ in the (x,y) plane (figure 19 iii)b and c), and corresponds to the positive peak of Φ at about $t \sim 6$ (figure 11 (a)). After $t \sim 7$ (note, $t = Rm = 8$ is the diffusion time), the alternating loops at $z \sim -2\pi, 0\pi$ and 2π are maintained and the magnitude of the field increases in the boundary layers. The prominent growth of the loops of wavelength 4π results from the nonlocal memory effect.

6 Concluding remarks

We have explicitly calculated a nonlocal and non-instantaneous generalization of the α effect for G.O. Roberts' flow. Separating the induction equation (1) into the mean part (2) and the fluctuating part (4) allows us to express the general kernel ϕ_{qr} of the electromotive force as a function of space and time. For $Rm \geq \mathrm{O}(1)$, nonlocalness and non-instantaneousness are apparent; they are clearly seen in the step response $\Phi(z,t)$. The response first grows on a timescale of the advection time τ_a. After that, it oscillates and approaches a steady state on a timescale of the diffusion time $\tau_\mathrm{d} = Rm\, \tau_\mathrm{a}$. For $Rm = 8$, a positive crest in $\Phi(z,t)$ at $t \sim 6$ extending from $|z| \sim \pi$ to $|z| \sim 3\pi$ is particularly noted, because it contributes to the enhancement in the growth rate of the mean field.

The temporal behaviour is visualized by a direct calculation of the time-development of field lines (figure 19). The helical flow twists the field line and makes it helical on a timescale of τ_a. After that, the field lines concentrate in the boundary layers and twisted loops spread in the z direction, manifesting nonlocalness. It should be interesting to compare this behaviour with direct numerical simulations of the geodynamo

(Kageyama and Sato 1997, Olson *et al.* 1999).

The nonlocal memory effect enables us to interpret the enhancement of the growth rate, seen in the dispersion relation of Roberts' kinematic dynamo. For $Rm = 8$, the peak in the response function at $(j, p) \sim (1/2, 1/6)$ is caused by a valley in the response function $\widetilde{\varphi}(j, p)$, a nonlocal and non-instantaneous generalization of the α-effect. The valley corresponds to the crest in $\Phi(z, t)$ at $t \sim 6$ around $|z| \sim 2\pi$. In this way, the response of the electromotive force consistently explains the form of the dispersion curve.

It is to be noted that the memory effect in this study operates even if the flow is steady. We have called it the 'magnetic memory', to distinguish it from the memory effect imparted by a finite correlation time of turbulence. We have called the latter the 'kinetic memory effect'. It may seem that our memory effect is similar to the 'transient effect' in Livermore and Jackson (2006) because the timescales are similar. The transient effect is an apparent amplification of the magnetic field due to the non-orthogonal superposition of the decaying eigenvectors (Schmid and Henningson 2001). Although our memory effect is transient in the sense that it eventually becomes steady, the two effects are different: the memory effect is a response to a source field, whereas the transient effect is independent of the source field.

Acknowledgments – We thank Professor Sei-ichiro Watanabe and two anonymous reviewers for helpful comments. This study was partly supported by the 21st Century COE Program "Dynamics of the Sun–Earth–Life Interactive System (SELIS)" of Nagoya University, the Inoue Foundation for Science and Center for Computational Astrophysics, CfCA, of National Astronomical Observatory of Japan. A part of the numerical computations were carried out on general common use computer system at CfCA. Data visualization of figure 19 was carried out on general common use computer system at the Information Technology Center, Nagoya University.

REFERENCES

Anufriyev, A.P. and Fishman, V.M., Magnetic field structure in the two-dimensional motion of a conducting fluid. *Geomag. Aeron.*, 1982, **22**, 245–248.

Brandenburg, A. and Sokoloff, D., Local and nonlocal magnetic diffusion and alpha-effect tensors in shear flow turbulence. *Geophys. Astrophys. Fluid. Dyn.,* , 2002, **96**, 319–344.

Busse, F.H., Thermal instabilities in rapidly rotating systems. *J. Fluid. Mech.,* , 1970, **44**, 441–460.

Busse, F.H., Convective flows in rapidly rotating spheres and their dynamo action. *Phys. Fluids.,* , 2002, **14**, 1301–1314.

Childress, S., Alpha-effect in flux ropes and sheets. *Phys. Earth Planet. Inter.,* , 1979, **20**, 172–180.

Courvoisier, A., Hughes, D.W. and Tobias, S.M., α Effect in a family of chaotic flows. *Phys. Rev. Lett.,* , 2006, **96**, 034503/1–4.

Desjardins, B., Dormy, E., Gilbert, A. and Proctor, M., Introduction to self-excited dynamo action. In *Mathematical Aspects of Natural Dynamos*, edited by E. Dormy and A.M. Soward, 2007, 3–57 (CRC Press: Boca Raton).

Fedotov, S., Ivanov, A. and Zubarev, A., Memory effects in a turbulent dynamo: Generation and propagation of a large-scale magnetic field. *Phys. Rev. E.,* 2002, **65**, 036313/1–5.

Fedotov, S., Ivanov, A. and Zubarev, A., Non-local mean field dynamo theory and magnetic fronts in galaxies. *Geophys. Astrophys. Fluid. Dyn.,* 2003, **97**, 135–148.

Kageyama, A. and Sato, T., Generation mechanism of a dipole field by a magnetohydrodynamic dynamo. *Phys. Rev. E.,* 1997, **55**, 4617–4626.

Käpylä, P.J., Korpi, M.J., Ossendrijver, M. and Stix, M., Magnetoconvection and dynamo coefficients III. α-effect and magnetic pumping in the rapid rotation regime. *Astron. Astrophys.,* , 2006, **455**, 401–412.

Kowal, G., Otmianowska-Mazur, K. and Hanasz, M., Dynamo coefficients in Parker unstable disks with cosmic rays and shear – The new methods of estimation. *Astron. Astrophys.,* 2006, **445**, 915-929.

Krause, F. and Rädler, K.-H., *Mean-field Magnetohydrodynamics and Dynamo Theory*, 1980 (Akagemie-Verlag: Berlin, and Pergaman Press: Oxford).

Livermore, P.W. and Jackson, A., Transient magnetic energy growth in spherical stationary flows. *Proc. R. Soc. A*, 2006, **462**, 2457–2479.

Matsushima, M., A scale-similarity model for the subgrid-scale flux with application to MHD turbulence in the Earth's core. *Phys. Earth Planet. Inter.,* 2005, **153**, 74–82.

Moffatt, H.K., *Magnetic Field Generation in Electrically Conducting Fluids*, 1978 (Cambridge University Press: Cambridge).

Müller, U. and Stieglitz, R., The Karlsruhe dynamo experiment. *Nonlinear Processes in Geophys.*, 2002, **9**, 165–170.

Olson, P., Christensen, U. and Glatzmaier, G.A., Numerical modeling of the geodynamo: Mechanisms of field generation and equilibration. *J. Geophys. Res.,* , 1999, **104**, 10383–10404.

Plunian, F. and Rädler, K.-H., Subharmonic dynamo action in the Roberts flow. *Geophys. Astrophys. Fluid. Dyn.,* 2002a, **96**, 115–133.

Plunian, F. and Rädler, K.-H., Harmonic and subharmonic solutions of the Roberts dynamo problem. Application to the Karlsruhe experiment. *magnetohydrodynamics*, 2002b, **38**, 92–103.

Rädler, K.-H., Apstein, E. and Schuler, M., The α-effect in the Karlsruhe dynamo experiment. *Proceedings of the 3rd International Conference "Transfer Phenomena in Magnetohydrodynamic and Electroconducting Flows"*, Vol.I, Aussois, France, 1997, 9–14.

Rädler, K.-H., The generation of cosmic magnetic fields. In *From the Sun to the Great Attractor, 1999 Guanajuato Lectures on Astrophysics*, edited by D. Page and J. Hirsch, 2000, 101–172 (Springer: Berlin).

Rädler, K.-H., Rheinhardt, M., Apstein, E. and Fuchs, H., On the mean-field theory of the Karlsruhe dynamo experiment. *Nonlin. Proc. Geophys.,* , 2002, **9**, 171–187.

Rädler, K.-H. and Brandenburg, A., Contributions to the theory of a two-scale homogeneous dynamo experiment. *Phys. Rev. E.,* , 2003, **67**, 026401/1–11.

Roberts, G.O., Dynamo action of fluid motions with two-dimensional periodicity. *Phil. Trans. Roy. Soc. London Ser. A*, 1972, **271**, 411–454.

Roberts, P.H., Kinematic dynamo models. *Phil. Trans. Roy. Soc. London Ser. A*, 1972, **272**, 663–698.

Roberts, P.H., Fundamentals of dynamo theory. In *Lectures on Solar and Planetary Dynamos*, edited by M.R.E. Proctor and A.D.Gilbert, 1994, 1–58 (Cambridge University Press: Cambridge).

Schmid, P.J. and Henningson D.S., *Stability and Transition in Shear Flows*, 2001, (Springer: New York).

Schrinner, M., Rädler, K.-H., Schmitt, D., Rheinhardt, M. and Christensen, U., Mean-field view on rotating magnetoconvection and a geodynamo model. *Astron. Nachr.,* 2005, **326**, 245–249.

Schrinner, M., Rädler, K.-H., Schmitt, D., Rheinhardt, M. and Christensen, U., Mean-field concept and direct numerical simulations of rotating magnetoconvection and the geodynamo, *Geophys. Astrophys. Fluid. Dyn.,* 2007, **101**, 81–116.

Soward, A.M., Fast dynamo action in a steady flow. *J. Fluid. Mech.,* 1987, **180**, 267-295.

Soward, A.M., On dynamo action in a steady flow at large magnetic Reynolds number. *Geophys. Astrophys. Fluid. Dyn.,* , 1989, **49**, 3-22.

Steenbeck, M., Krause, F. and Rädler, K.-H., A calculation of the mean electromotive force in an electrically conducting fluid in turbulent motion, under the influence of Coriolis forces. *Z.Naturforsch.,* 1966, **21**a, 369-376 [English transl.: Roberts and Stix *The Turbulent Dynamo: A translation of a series of papers by F. Krause, K.-H. Rädler, and M. Steenbeck,* pp.29-47, 1971 (NCAR: Boulder).].

Steenbeck, M. and Krause, F., The generation of stellar and planetary magnetic fields by turbulent dynamo action. *Z.Naturforsch.,* 1966, **21**a, 1285–1296 [English translation: Roberts and Stix, *The Turbulent Dynamo: A translation of a series of papers by F. Krause, K.-H. Rädler, and M. Steenbeck,* 49–79, 1971 (NCAR: Boulder).].

Stieglitz, R. and Müller, U., Experimental demonstration of a homogeneous two-scale dynamo. *Phys. Fluids.,* 2001, **13**, 561–564.

Tilgner, A. and Busse, F.H., Subharmonic dynamo action of fluid motions with two-dimensional periodicity. *Proc. R. Soc. Lond. A*, 1995, **448**, 237–244.

Tobias, S. and Weiss, N., The solar dynamo and the tachocline. In *The Solar Tachocline*, edited by D.W. Hughes, R. Rosner, N.O. Weiss, 2007, 319–350 (Cambridge University Press: Cambridge).

Urpin, V., Mean electromotive force in turbulent shear flow. *Phys. Rev. E.,* 2002, **65**, 026301/1–8.

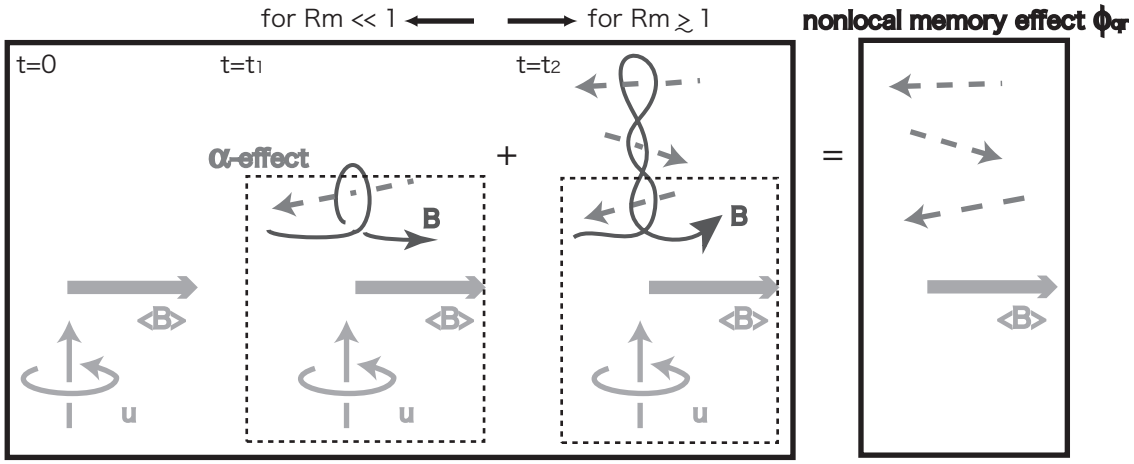

Figure 1. Schematic illustration of the generation of the nonlocal memory effect showing the time evolution of a magnetic line of force in a helical velocity field $\mathbf{u}$. The initial field line is straight and can be represented as $\langle \mathbf{B} \rangle$. The helical flow first warps the field line and then twists it by 90 degrees, generating an electromotive force locally around the mean field ($t = t_1$). This is the well-known α-effect. For small Rm, the twist remains steady with time because magnetic diffusion is effective. If $Rm \gtrsim 1$, the distortion of the field lines increases with time ($t = t_2$), generating an electromotive force which varies in time and space. This behaviour necessitates extending the expression of the α-effect to a nonlocal and non-instantaneous function ϕ_{qr}.

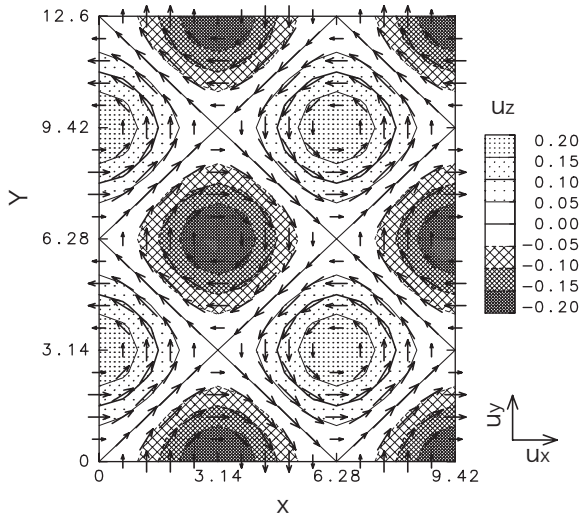

Figure 2. The flow of G.O.Roberts (1972). The vectors represent a two-dimensional velocity field (u_x, u_y) and the grey scale represents the magnitude of u_z. The flow consists of helical columns with axes in the z direction. It is two-dimensionally periodic on the (x, y) plane with a period of $2\pi \times 2\pi$.

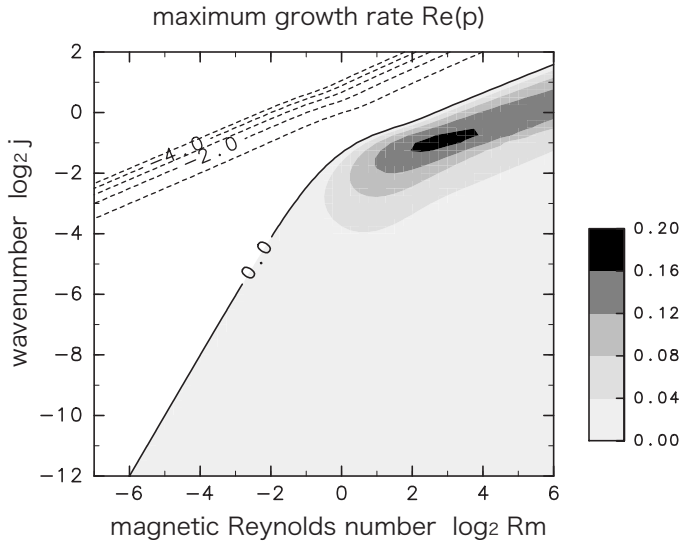

Figure 3. Maximum growth rate Re[p] of the kinematic dynamo of G.O.Roberts (1972). The grey scale represents the magnitude of the positive Re[p]. The dashed contours represent the magnitude of Re[p] in the range of $-5 \leq \mathrm{Re}[p] \leq 0$ with an interval of 1.0 . The growth rate Re[p] is positive for any Rm if the wavenumber j is small enough. It has a peak along $j \sim Rm^{0.3}$ for $Rm \gtrsim 1$ and the fastest growth rate for all Rm is Re[p] ~ 0.17 at $j \sim 0.5$ for $Rm = 8$.

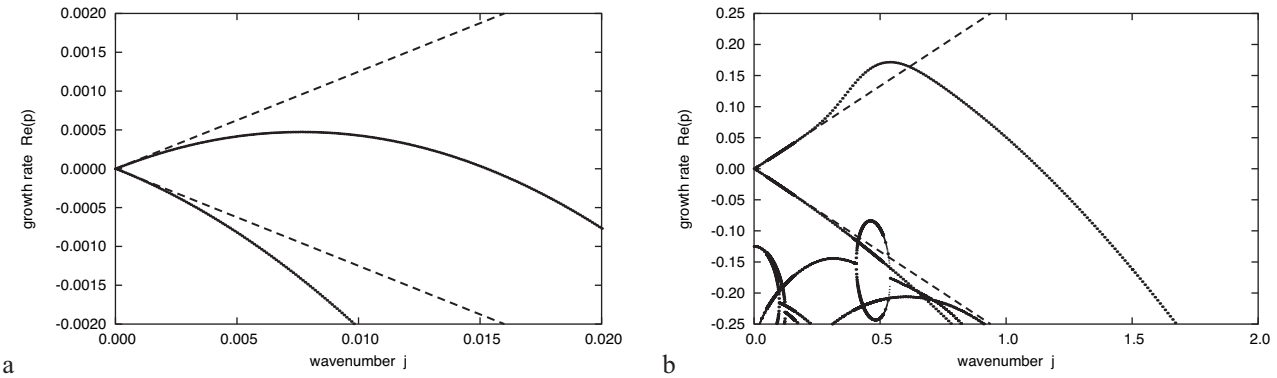

Figure 4. Dispersion relations of Roberts' kinematic dynamo for (a) $Rm = 1/8$ and (b) $Rm = 8$. The dotted curves represent the dispersion relations and the dashed lines represent those expected for traditional local α-effects defined by (48) or (49) without the β-effect. Whereas the dynamo for $Rm = 1/8$ does not grow faster than that produced only by the α-effect, that for $Rm = 8$ grows faster than that produced only by the α-effect at around $j \sim 1/2$.

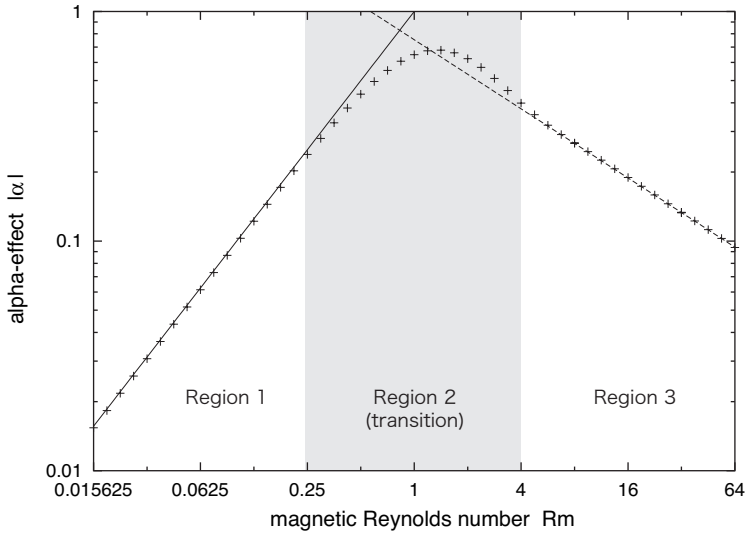

Figure 5. Absolute value of α defined as (48) or (49) versus the magnetic Reynolds number. The crosses represent $|\alpha|$, estimated from $p^*(j)/j$ at $j = 1/64$, where p^* is the modified eigenvalue (36) of the growing branch. The solid and dashed lines are analytical asymptotic approximations for $Rm \ll 1$ (53) and $Rm \gg 1$ (54), respectively.

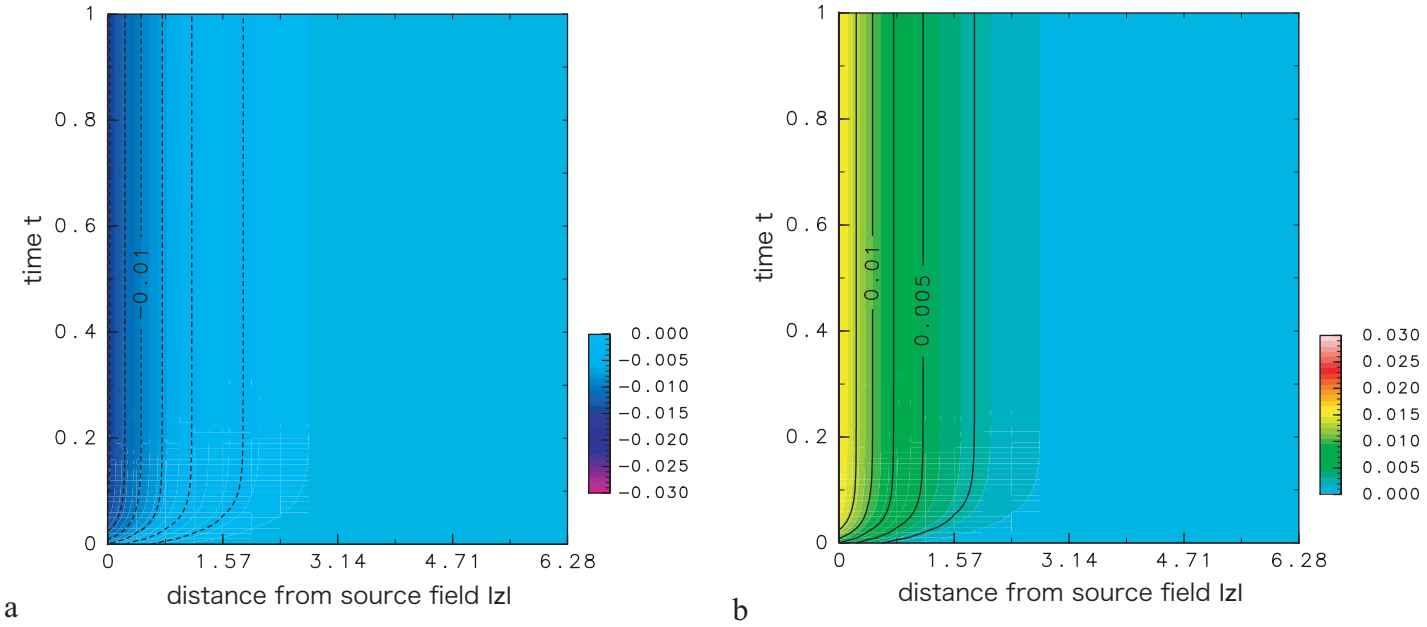

Figure 6. Contours of (a) Φ and (b) Ψ in (z, t) space for $Rm = 1/32$. The horizontal axis is the distance $|z|$ from the plane where the source field $\langle \mathbf{B} \rangle$ is placed. The vertical axis is the time t since the source field is set. The dashed and thin solid contours and colours visible in the electronic version represent their strength (the dashed and solid curves represent negative and positive values, respectively). The interval of the dashed and solid contours is 0.0025. Both Φ and Ψ are generated until $t \sim Rm = 1/32$ and remain steady after that.

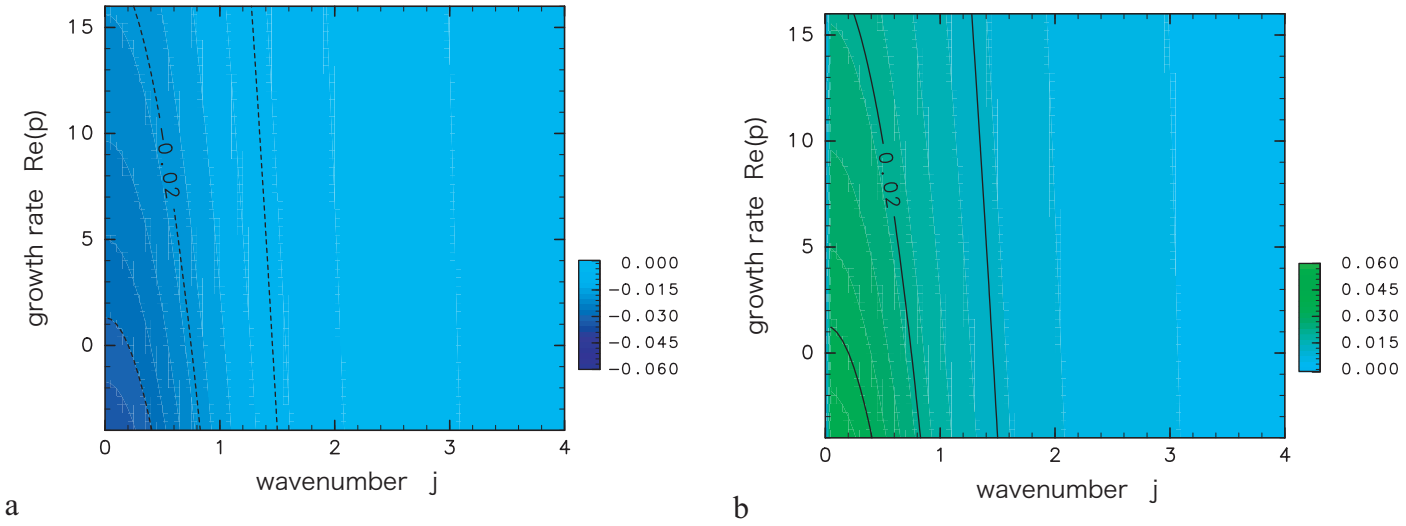

Figure 7. Contours of (a) $\widetilde{\varphi}$ and (b) $\widetilde{\psi}$ in (j,p) space for $Rm = 1/32$. The dashed and thin solid contours and colours visible in the electronic version represent their strength (the dashed and solid curves represent negative and positive values, respectively). The interval of the dashed and solid contours is 0.01. The kernels $\widetilde{\varphi}$ and $\widetilde{\psi}$ are almost independent of p. The decay of $\widetilde{\varphi}$ and $\widetilde{\psi}$ with increasing j results from magnetic diffusion.

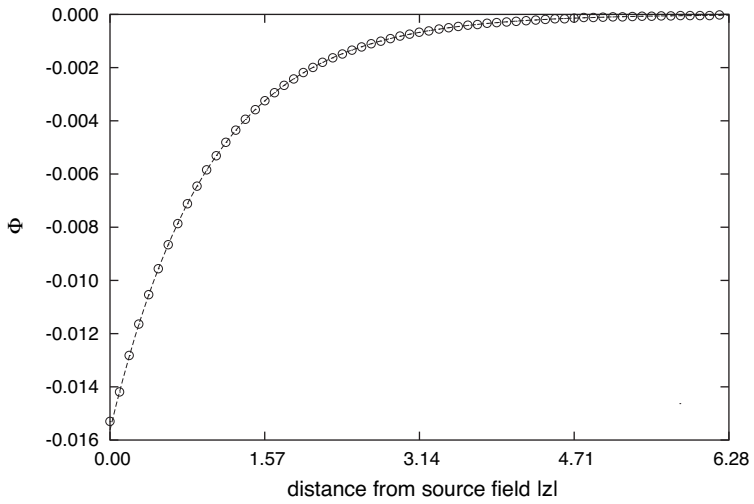

Figure 8. Comparison of the numerical values [circles] of $\Phi(|z|, t = 1.0)$ with its analytic approximation (64) [dashed line] for $Rm = 1/32$. The horizontal axis is the distance from the $z = 0$ plane.

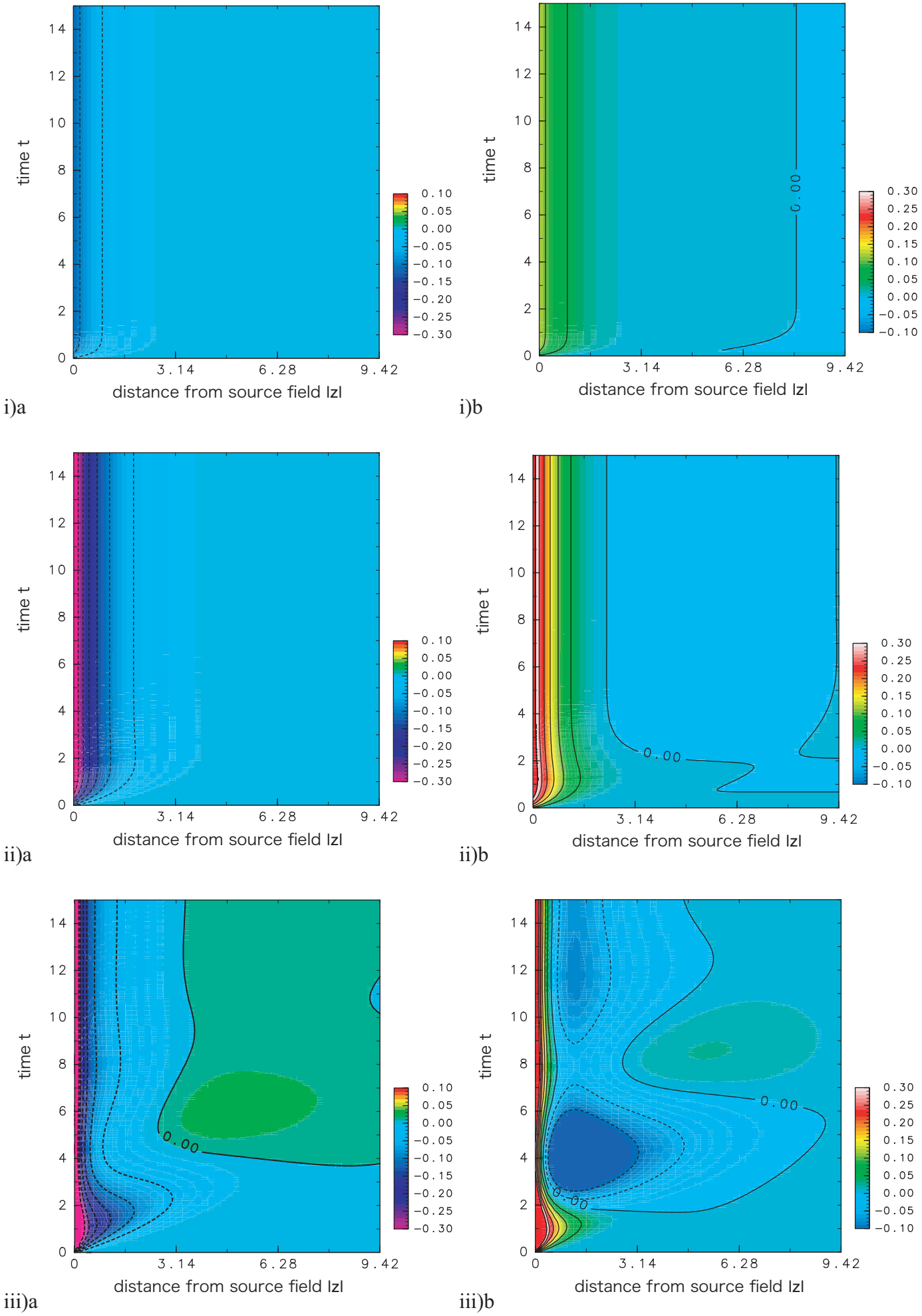

Figure 9. Contours of (a) Φ and (b) Ψ in (z,t) space for (i) $Rm = 1/4$, (ii) $Rm = 1$ and (iii) $Rm = 4$ with axes as in figure 6 but with a different colour scale. The interval of the dashed and solid contours is 0.05. Nonlocalness and non-instantaneousness increase with Rm.

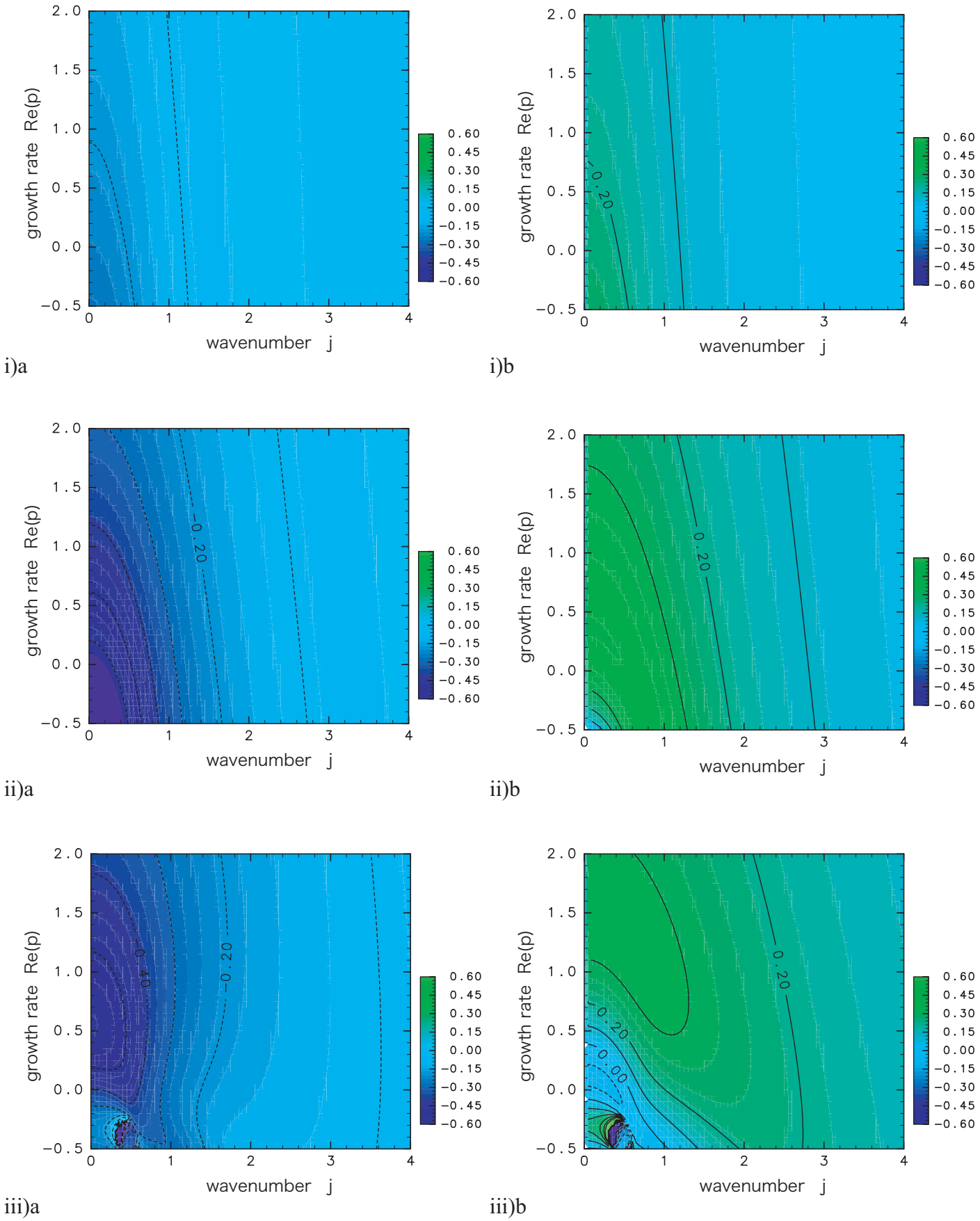

Figure 10. Contours of (a) $\widetilde{\varphi}$ and (b) $\widetilde{\psi}$ in (j,p) space for (i) $Rm = 1/4$, (ii) $Rm = 1$ and (iii) $Rm = 4$ with axes as in figure 7 but with a different colour scale. The interval of the dashed and solid contours is 0.1.

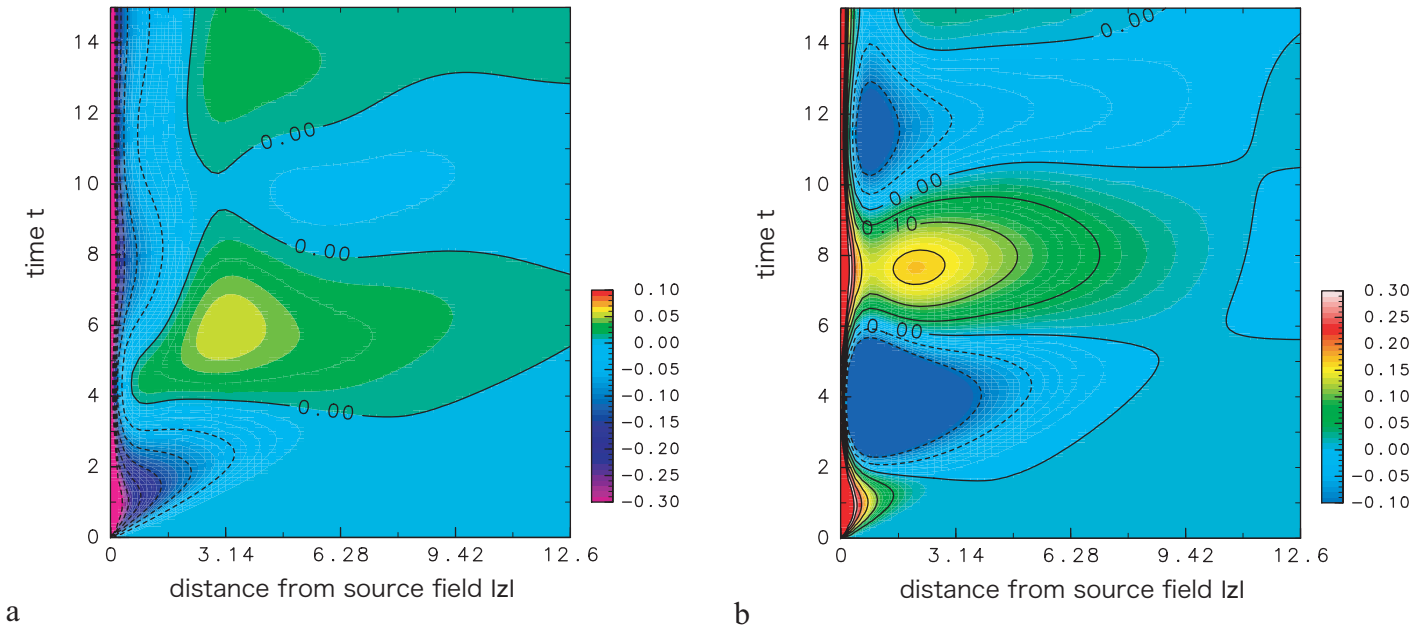

Figure 11. Contours of (a) Φ and (b) Ψ in (z,t) space for $Rm = 8$, with axes and colours as in figure 6 but with a different colour scale. The interval of the dashed and solid contours is 0.05. Note that Φ and Ψ for $Rm = 8$ spread with time in the $|z|$ direction at first and then oscillate with time. A positive peak of Φ exists at around $t \sim 6$ and $|z| \sim \pi$.

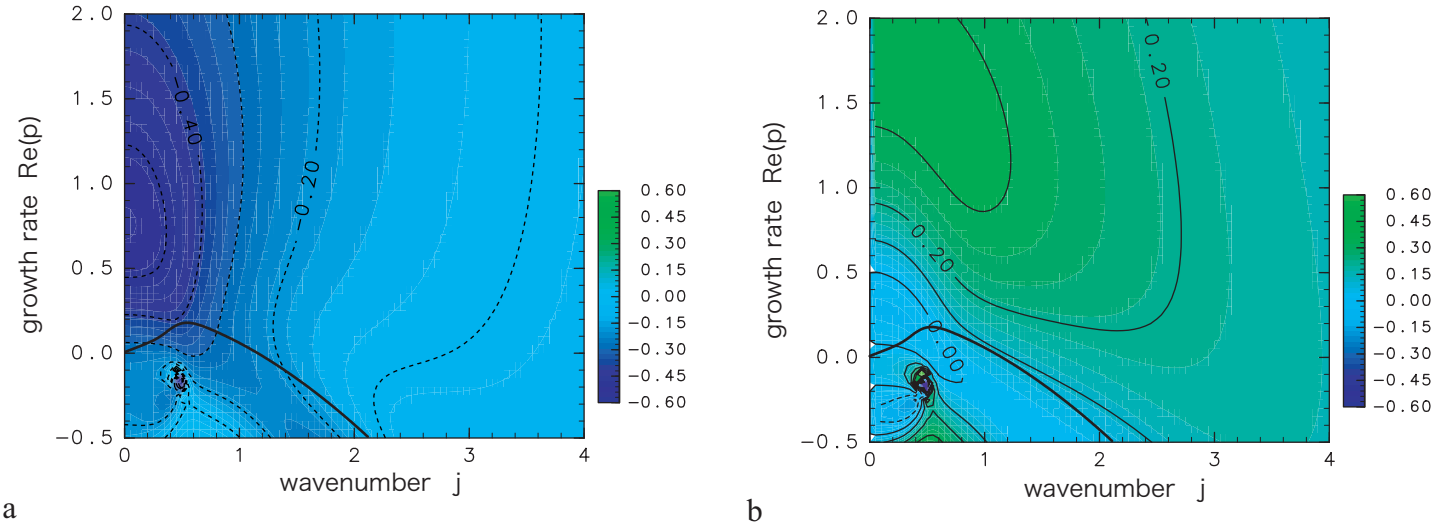

Figure 12. Contours of $\widetilde{\varphi}$ and $\widetilde{\psi}$ in (j,p) space for $Rm = 8$, with axes, colours and lines as in figure 7 but with different scales. The interval of the dashed and solid contours is 0.1. The thick solid lines represent the dispersion relation of the fastest growing branch. The responses $\widetilde{\varphi}$ and $\widetilde{\psi}$ depend strongly on j and p.

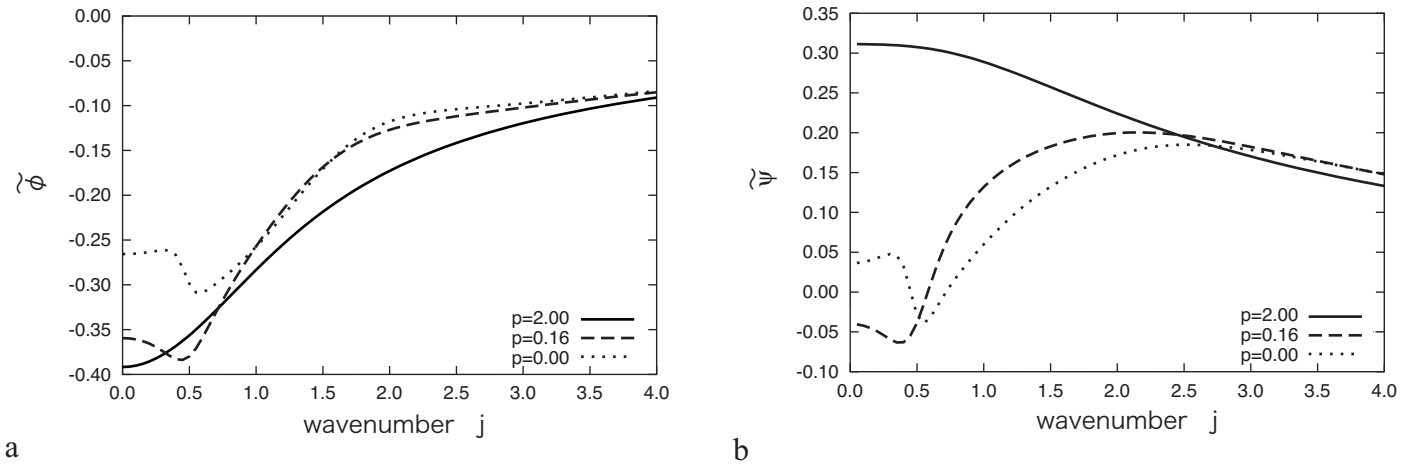

Figure 13. (a) $\widetilde{\varphi}$ and (b) $\widetilde{\psi}$ versus wavenumber j for three values of p for $Rm = 8$. The solid, dashed and dotted curves represent $\widetilde{\varphi}$ and $\widetilde{\psi}$ at $p = 2.0$, 0.16 and 0.0, respectively. The diagonal kernel $\widetilde{\varphi}$ is always negative and has a peak at $j \sim 1/2$ for $p = 0.16(\sim 1/6)$. The off-diagonal kernel $\widetilde{\psi}$ is positive for large p, but has a negative peak at $j \sim 1/2$ for $p \sim 1/6$.

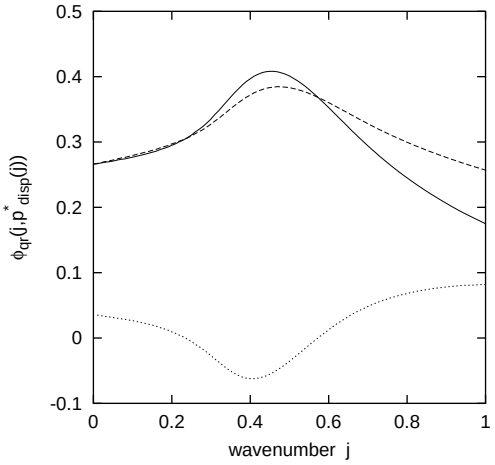

Figure 14. Extended α-effect [solid curve] defined as $\hat{\alpha}(j) = |\widetilde{\varphi}(j, p_{\rm disp}(j))| - j\widetilde{\psi}(j, p_{\rm disp}(j))$, where $p = p_{\rm disp}(j)$ is the Roberts' dispersion relation, for $Rm = 8$. The dashed and dotted curves represent $\widetilde{\varphi}$ and $\widetilde{\psi}$, respectively.

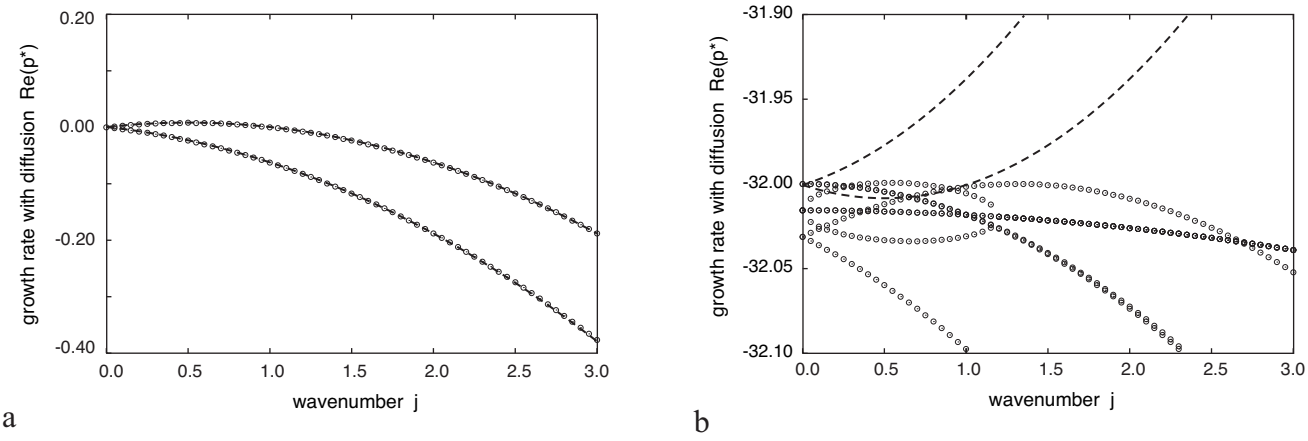

Figure 15. Comparison of the numerical dispersion relation [circles] of Roberts' kinematic dynamo with our analytic solutions (70) [dashed curves] for $Rm = 1/32$. The horizontal axis is the wavenumber and the vertical axis is the modified growth rate Re$[p^*]$. The upper and lower branches in (a) are the horizontally uniform growing and decaying solutions, respectively, both of which are generated by the α^2-mechanism. The two branches of the analytic solutions with $p^* \sim -1/Rm$ (b) are spurious.

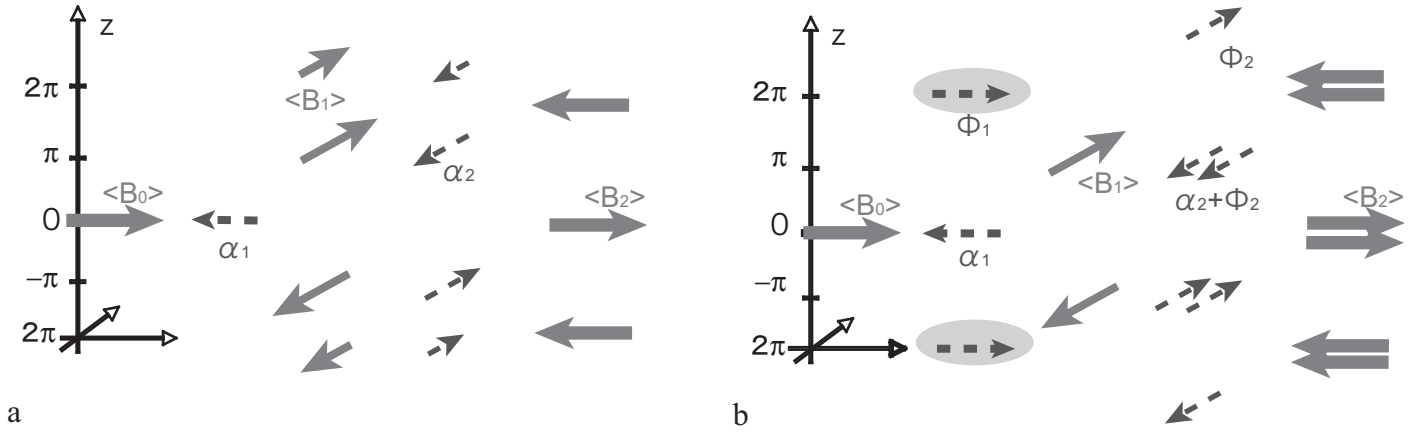

Figure 16. Schematic diagram of the generating mechanisms of the mean field (a) for $Rm < 1/4$ and (b) for $Rm \gtrsim 4$. The vertical axis represents the z direction and corresponds to the horizontal axes in figures 6 and 11. For $Rm \gtrsim 4$, a nonlocal Φ_1 with a dominant wavenumber of $j \sim 1/2$ is generated in addition to the local component α, inducing the mean field $\langle \mathbf{B}_1 \rangle$ which grows with wavenumber $j \sim 1/2$.

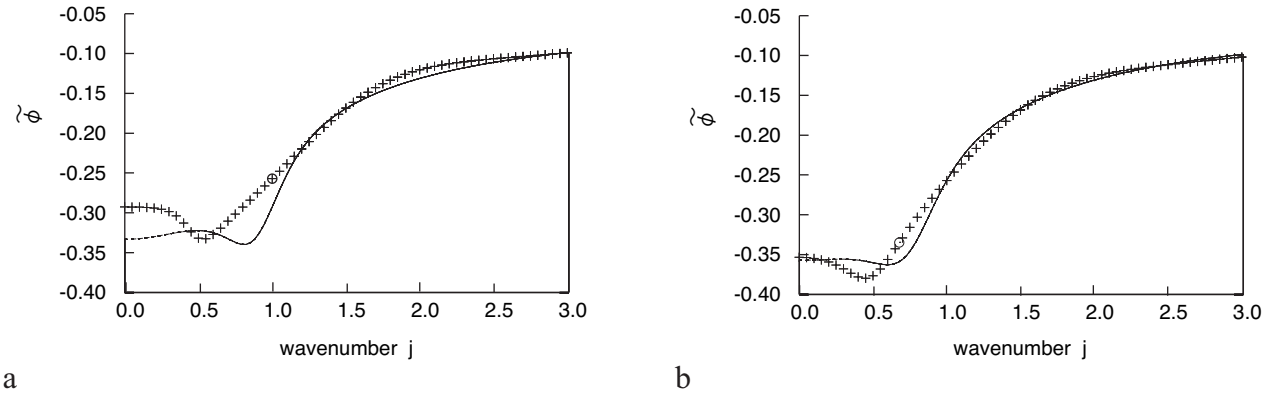

Figure 17. Comparisons of the numerical values of $\widetilde{\varphi}$ [crosses] and the approximated form (76) [dashed curves] for $Rm = 8$ at (a) $p = 0.05$ and (b) $p = 0.15$. The open circles represent the positions of the intersections with the numerical dispersion curve of Roberts' kinematic dynamo.

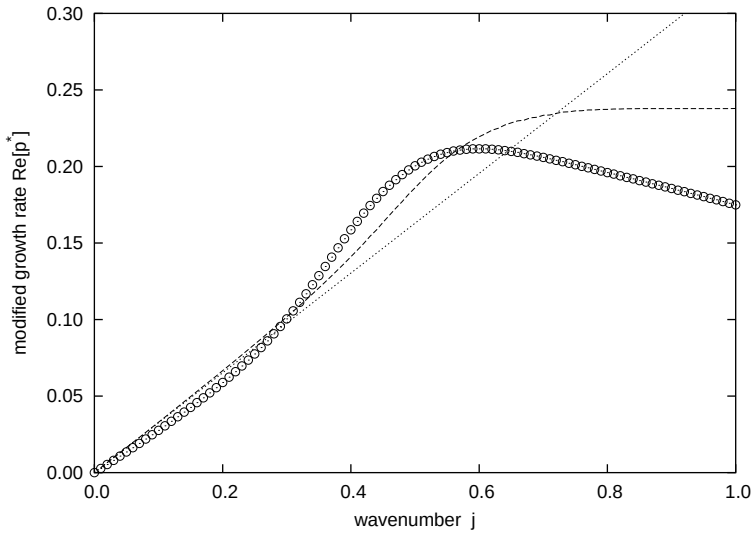

Figure 18. Comparison of the numerical dispersion relation of Roberts' kinematic dynamo [circles] with our approximated solutions derived from (76) under the assumption $\widetilde{\psi} = 0$ [dashed curve] for $Rm = 8$. The horizontal axis is the wavenumber and the vertical axis is the modified growth rate Re[p^*]. The dotted line represents the dispersion relation produced by (76) with $j = p = 0$.

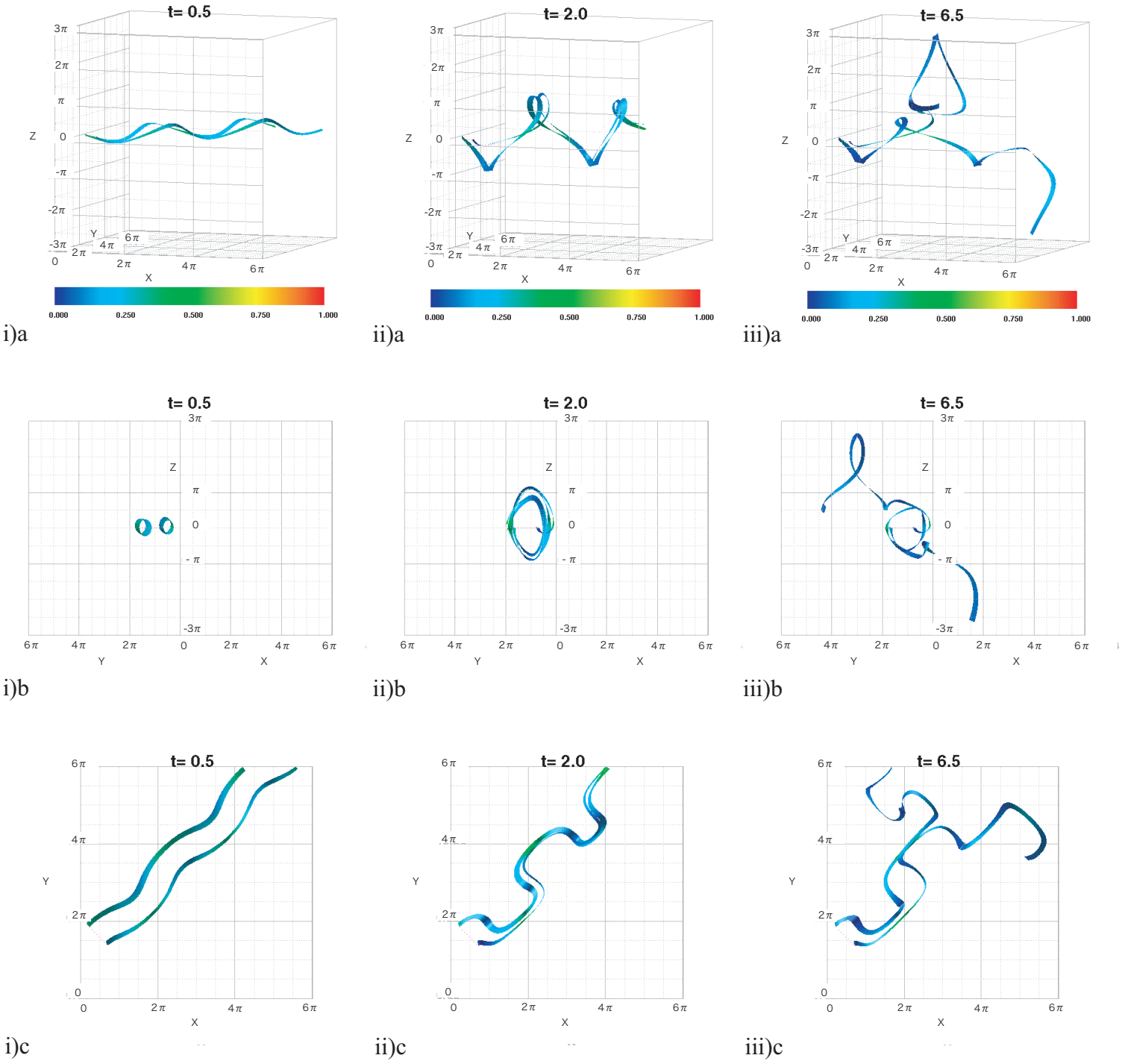

Figure 19. Time evolution of the magnetic lines of force for $Rm = 8$. Two field lines passing through $(0.78, 5.81, 0.0)$ and $(2.15, 4.44, 0.0)$ are shown at (i) $t = 0.5$, (ii) 2.0 and (iii) 6.5. We calculated the induction equation (1) for Roberts' flow (9) in a box of dimensions $6\pi \times 6\pi \times 6\pi$. The initial field is $\langle \mathbf{B} \rangle = (1, 1, 0)\delta(z)$. We use a periodic boundary condition in the x and y directions, and $\mathbf{B}$ is forced to vanish at $z = -3\pi$ and 3π. Views from three directions are placed from top to bottom: [a] views from the direction $(-0.15, 0.98, -0.14)$ [b] views from the direction of the initial field, $(1, 1, 0)$ and [c] projections onto the (x, y) plane.

Appendix A: Numerical method

This section explains the method of calculating $\widetilde{\varphi}, \widetilde{\psi}, \Phi$ and Ψ. First, (25) is used to calculate the fluctuation field $\mathbf{H}'$. The calculation method is different for the two sets $\{\widetilde{\varphi}, \widetilde{\psi}\}$ and $\{\Phi, \Psi\}$. For the set $\{\widetilde{\varphi}, \widetilde{\psi}\}$, we calculate (25) in (j,p) space for a source field $\langle\mathbf{H}\rangle$ to obtain $\mathbf{H}'(x,y,j,p)$. The set $\{\Phi, \Psi\}$ is calculated in (j,t) space for a source field $\langle\widetilde{\mathbf{B}}\rangle = \langle\widetilde{\mathbf{B}_0}\rangle\Theta(t)$ to obtain $\mathbf{H}'(x,y,j;t)$. The discretization methods for the calculations above are described later. Next, (19) is used to obtain $\widetilde{\boldsymbol{\mathcal{E}}}(j,p)$ for $\{\widetilde{\varphi}, \widetilde{\psi}\}$, and $\widetilde{\boldsymbol{\mathcal{E}}}(j;t)$ for $\{\Phi, \Psi\}$. Finally, the set of the responses $\{\widetilde{\varphi}, \widetilde{\psi}\}$ is determined from (33), or

$$\begin{pmatrix} \widetilde{\mathcal{E}}_x \\ \widetilde{\mathcal{E}}_y \end{pmatrix} = \begin{pmatrix} \widetilde{\varphi}(|j|,p) & \mathrm{i}j\widetilde{\psi}(|j|,p) \\ -\mathrm{i}j\widetilde{\psi}(|j|,p) & \widetilde{\varphi}(|j|,p) \end{pmatrix} \begin{pmatrix} \langle H_x\rangle \\ \langle H_y\rangle \end{pmatrix}. \tag{A1}$$

On the other hand, the set of the responses $\{\Phi, \Psi\}$ is obtained in two steps. First $\{\widetilde{\Phi}(|j|;t), \widetilde{\Psi}(|j|,t)\}$ is calculated from

$$\begin{pmatrix} \widetilde{\mathcal{E}}_x(|j|;t) \\ \widetilde{\mathcal{E}}_y(|j|;t) \end{pmatrix} = \begin{pmatrix} \widetilde{\Phi}(|j|;t) & \mathrm{i}j\widetilde{\Psi}(|j|;t) \\ -\mathrm{i}j\widetilde{\Psi}(|j|;t) & \widetilde{\Phi}(|j|;t) \end{pmatrix} \begin{pmatrix} \langle\widetilde{B}_0\rangle_x \\ \langle\widetilde{B}_0\rangle_y \end{pmatrix} \quad (t>0). \tag{A2}$$

Then inverse Fourier transforms of $\widetilde{\Phi}(j;t)$ and $\widetilde{\Psi}(j;t)$ are performed to obtain $\Phi(z,t)$ and $\Psi(z,t)$ in (z,t) space. As is evident from the equations above, the source fields $\langle\mathbf{H}\rangle = (1,0)$ and $\langle\widetilde{\mathbf{B}}_0\rangle = (1,0)$ provide sufficient information to calculate $\{\widetilde{\varphi}, \widetilde{\psi}\}$ and $\{\Phi, \Psi\}$, respectively.

We use the following discretization of (25) to calculate $\widetilde{\varphi}$ and $\widetilde{\psi}$ in (j,p) space. Since the perturbation field $\mathbf{H}'$ is periodic in x and y, it can be expanded in the Fourier series

$$\mathbf{H}'(x,y,j,p) = \sum_{m=-m_s}^{+m_s} \sum_{n=-n_s}^{+n_s} \mathbf{h}_{mn}(j,p)\mathrm{e}^{\mathrm{i}mx}\mathrm{e}^{\mathrm{i}ny}, \tag{A3}$$

where m and n are integers and m_s and n_s are the truncation degrees. Equation (25) can be Fourier-expanded accordingly to become

$$\begin{aligned} &\{p^* + Rm^{-1}(m^2+n^2)\}\mathbf{h}_{mn} + \frac{1}{2}(m\mathbf{h}_{m,n-1} - m\mathbf{h}_{m,n+1} + n\mathbf{h}_{m-1,n} - n\mathbf{h}_{m+1,n}) \\ &\qquad - \frac{1}{2}\begin{pmatrix} h_{y,m(n-1)} + h_{y,m(n+1)} \\ h_{x,(m-1)n} + h_{x,(m+1)n} \\ \mathrm{i}(h_{x,(m-1)n} - h_{x,(m+1)n} - h_{y,m(n-1)} + h_{y,m(n+1)}) \end{pmatrix} \\ &\qquad + \frac{1}{2}\mathrm{i}j(\mathbf{h}_{m-1,n} + \mathbf{h}_{m+1,n} - \mathbf{h}_{m,n-1} - \mathbf{h}_{m,n+1}) \\ &\qquad + \frac{1}{2}\mathrm{i}j\begin{pmatrix} -(h_{x,-10} + h_{x,10} - h_{x,0-1} - h_{x,01}) - \mathrm{i}(h_{z,0-1} - h_{z,01}) \\ -\mathrm{i}(h_{z,-10} - h_{z,10}) - (h_{y,-10} + h_{y,10} - h_{y,0-1} - h_{y,01}) \\ 0 \end{pmatrix} = \mathbf{r}_{mn}, \end{aligned} \tag{A4}$$

where $\mathbf{r}_{mn}$ are the coefficients of the Fourier series of the right-hand sides of (25) and are given by

$$\begin{aligned}
\mathbf{r}_{1,0} &= \frac{1}{2}\begin{pmatrix} -\mathrm{i}j & 0 \\ 1 & -\mathrm{i}j \\ \mathrm{i} & 0 \end{pmatrix}\begin{pmatrix} \langle H_x\rangle \\ \langle H_y\rangle \end{pmatrix}, \quad \mathbf{r}_{-1,0} = \frac{1}{2}\begin{pmatrix} -\mathrm{i}j & 0 \\ 1 & -\mathrm{i}j \\ -\mathrm{i} & 0 \end{pmatrix}\begin{pmatrix} \langle H_x\rangle \\ \langle H_y\rangle \end{pmatrix}, \\
\mathbf{r}_{0,1} &= \frac{1}{2}\begin{pmatrix} \mathrm{i}j & 1 \\ 0 & \mathrm{i}j \\ 0 & -\mathrm{i} \end{pmatrix}\begin{pmatrix} \langle H_x\rangle \\ \langle H_y\rangle \end{pmatrix}, \quad \mathbf{r}_{0,-1} = \frac{1}{2}\begin{pmatrix} \mathrm{i}j & 1 \\ 0 & \mathrm{i}j \\ 0 & \mathrm{i} \end{pmatrix}\begin{pmatrix} \langle H_x\rangle \\ \langle H_y\rangle \end{pmatrix}, \\
\mathbf{r}_{mn} &= \mathbf{0} \quad \text{for the other } m \text{ and } n.
\end{aligned} \tag{A5}$$

We use the LINPACK code to solve the simultaneous equations (A4) of $\mathbf{h}_{mn}$.

Equation (A4) is modified to calculate $\mathbf{H}'(x,y,j;t)$ to obtain Φ and Ψ. The term including the growth rate $p\mathbf{h}_{m,n}$ is replaced by the time-derivative $\partial\mathbf{h}_{m,n}/\partial t$ to obtain the time development of $\mathbf{h}_{m,n}(j;t)$. The integration in time is carried out using the Euler scheme with a time step of $\Delta t = 5\times10^{-3}$. The initial condition is $\mathbf{H}' = \mathbf{0}$, or $\mathbf{h}_{m,n}(j;0) = \mathbf{0}$ for any m and n.

Once $\mathbf{h}_{m,n}$ is obtained, the electromotive force $\widetilde{\boldsymbol{\mathcal{E}}}$ induced by the fluctuating field $\mathbf{H}'$ or $\mathbf{h}_{m,n}$ is calculated from

$$\begin{pmatrix} \widetilde{\mathcal{E}}_x \\ \widetilde{\mathcal{E}}_y \\ \widetilde{\mathcal{E}}_z \end{pmatrix} = \langle \mathbf{u}\times\mathbf{H}'\rangle = \frac{1}{2}\begin{pmatrix} -\mathrm{i}(h_{z,-10} - h_{z,10}) - (h_{y,-10} + h_{y,10} - h_{y,0-1} - h_{y,01}) \\ (h_{x,-10} + h_{x,10} - h_{x,0-1} - h_{x,01}) + \mathrm{i}(h_{z,0-1} + h_{z,01}) \\ 0 \end{pmatrix}. \tag{A6}$$

The truncation degrees for calculating $\mathbf{H}'$ are $m_s = n_s = 9$ so that numerical values of $\widetilde{\varphi}$ and $\widetilde{\psi}$ should converge within 10^{-8} for $Rm \le 10$. For calculating $\widetilde{\Phi}(z,t)$ and $\widetilde{\Psi}(z,t)$, we use 321 j points: $0 \le j \le 32$ with the interval $\Delta j = 0.1$ for $Rm < 1/4$ and and $0 \le j \le 64$ with $\Delta j = 0.2$ for $1/4 \le Rm \le 10$. This guarantees convergence of $\Phi(z,t)$ and $\Psi(z,t)$ within 4%.

Appendix B: Derivation of (58)

When the fluctuating field $\mathbf{H}'$ and the right-hand term of (57) are expanded in the Fourier series defined by (A3), (57) reduces to

$$\left\{p^* + Rm^{-1}(m^2+n^2)\right\}\mathbf{h}_{m,n} = \mathbf{r}_{m,n}, \tag{B1}$$

where $\mathbf{r}_{m,n}$ is defined as (A5). Equation (B1) can be solved and Fourier-transformed to give

$$\mathbf{H}' = \sum_{m,n}\frac{1}{p^* + Rm^{-1}(m^2+n^2)}\mathbf{r}_{m,n}\mathrm{e}^{\mathrm{i}mx+\mathrm{i}ny}. \tag{B2}$$

When (A5) is substituted into $\mathbf{r}_{m,n}$ in the right-hand side, all the terms vanish apart from those with truncation degrees $(m,n) = (\pm1,0)$ or $(0,\pm1)$. Thus we obtain the form of (58).